CALIBRATION OF POWDER CONSTITUTIVE MODEL USING DIGITAL IMAGE CORRELATION VALIDATED FOR HOLLOW HEMISPHERE OF LEAD ZIRCONATE TITANATE

Mateus Mota Morais[a*]
Caiuã Caldeira de Melo[b]
Rodrigo Bresciani Canto[b]
Carlos Alberto Fortulan[a]

[a]Department of Mechanical Engineering, São Carlos School of Engineering, University of São Paulo, Trabalhador São-carlense, 400, São Carlos, 13566-590, Brazil
[b]Federal University of São Carlos (UFSCar), Department of Materials Engineering (DEMa), 13565-905 São Carlos, SP, Brazil

[*]Corresponding author at: Department of Mechanical Engineering, São Carlos School of Engineering, University of São Paulo, Trabalhador São-carlense, 400, São Carlos, 13566-590, Brazil.
E-mail: mateus.morais@usp.br

Accepted manuscript published at Powder Technology
DOI: https://doi.org/10.1016/j.powtec.2021.07.001

ABSTRACT

This paper presents the application of digital image correlation to uniaxial and diametral compression tests to identify the Drucker-Prager/cap shear failure and the elastic parameters of a lead zirconate titanate powder (PZT). The calibrated parameters were validated through finite element simulation of the cold isostatic pressing of a hollow hemisphere used in piezoelectric transducers. The results showed that the dilatancy stresses were 50-65% lower than the fracture stresses, demonstrating that adopting the fracture stress may overestimate material cohesion. The simulation using the calibrated model achieved an excellent agreement with the measured geometry, with a difference of only 1.1% in the dimension and 2.0% in the average density. The results highlight how digital image correlation can obtain more accurate parameters with

fewer tests. The proposed methodology can be used to calibrate other powder materials, especially those in which dilatancy plays a key role.

Keywords: Drucker-Prager/cap; Powder compaction; Finite element; Parameter Identification; PZT; Dilatancy

1. INTRODUCTION

The finite element (FE) method has been widely used in academia and industry to model compacted powder parts and optimize their production and handling [1–4]. When effectively used, FE simulations can predict the dimensions, shape, density distribution, and possible failure regions of compacted parts [3,5,6]. These simulations improve designing molds for powder pressing and planning subsequent steps such as green machining [3,6,7], thus obtaining compacted parts with correct dimensions and uniform density, reducing trial-and-error iterations [8]. Especially for brittle materials, such as ceramics, simulations are fundamental to indicate regions more susceptible to cracks caused by non-homogeneous density distribution or excessive shear stresses [9–11].

For powder-like materials, there are two possible modeling strategies: the discrete approach (which considers each particle and its interactions individually) and the phenomenological or continuum approach (which considers the powder as a continuum) [9]. The continuum approach is usually implemented in FE simulations as it requires less computational effort and is a valid assumption when the size of the compacted part is orders of magnitude larger than the particles [9]. One of the most used continuum constitutive models for granular-like materials is the Drucker-Prager/cap (DPC) model [12,13] that has been applied with success to the simulation of several materials, such as soil [14], wood chips [15], pharmaceutical excipients [4,6,7,16,17], cosmetics [18], metals [19–22], cemented carbides [23] graphite [8], and other ceramics [5,24].

However, due to its complexity, the DPC model requires the calibration of several parameters to obtain accurate and reliable simulations [2,24,25]. Some alternatives have been proposed to reduce the number and complexity of the calibration tests. For instance, many authors used inverse analysis, adjusting the model parameters to minimize the difference between the simulation and a simple test (such as uniaxial compaction in a closed die). The minimization problem could be solved by classical optimization algorithms [23,24,26], genetic algorithms [27,28], neural network [11], and even a manual "trial-and-error" calibration [21].

However, there are some limitations to the optimization approach. First, it requires some previous knowledge about the limits of the parameters, which might be unavailable for new or uncharacterized materials. For instance, there is no information about the calibration of lead zirconate titanate (PZT) powder with the DPC model. Second, due to the large number of parameters of the DPC model, multivariable optimization can result in an unrealistic set of parameters that do not represent the material behavior in experimental conditions different from the calibration. For example, Zhou et al. [26] used inverse analysis and obtained a set of parameters that accurately represented the material behavior during the loading stage but failed to represent it during unloading.

A promising solution to minimize the calibration challenges is through digital image correlation (DIC), a non-contacting full-field measurement based on acquiring pictures of a sample throughout an experiment [29–32]. Considered very versatile, DIC has been widely adopted in diverse applications in the last twenty years, including identifying parameters of constitutive models [30–32]. One of the significant advantages of the DIC is to obtain a full-field displacement measurement instead of the average displacement, hence obtaining more information from a calibration test, which can reduce the number and complexity of required calibration experiments.

This paper presents the application of DIC to calibrate the DPC model for lead zirconate titanate (PZT) powder, highlighting the advantages of its use, especially identifying the material dilatancy. The calibrated model was validated by comparing the dimensions and density of a hollow PZT hemisphere (a piezoelectric component used in acoustic transducers) obtained by cold isostatic pressing with the FE simulation of the compaction.

2. CONSTITUTIVE MODEL AND CALIBRATION ALTERNATIVES

2.1. The Drucker-Prager/cap constitutive model.

The DPC model used herein is defined by three yield surfaces (Figure 1): a linear shear failure surface [12,13], an elliptical cap yield surface that governs material densification [12,33], and a smooth transition surface to facilitate numerical implementation [12]. If the stress state on the material reaches the cap yield surface, the material undergoes plastic compaction, increasing its density and expanding the cap yield surface (hardening) [9,12,16,34]. Conversely, if the stress state reaches the shear failure surface, the material undergoes plastic volumetric

expansion (also known as dilation or dilatancy) [13], contracting the cap yield surface (softening) [9,12,16].

The shear failure, elliptical cap, and transition yield surfaces are defined by Equations 1, 2, and 3, respectively, which relate the Mises equivalent stress, *q*, with the equivalent pressure stress, *p* (negative of the first invariant of the stress tensor) [12]. Several parameters are required to define the plasticity model: material cohesion, *d*, material internal friction angle, *β*, cap eccentricity parameter (ratio of the elliptical axis), *R*, and the transition surface radius parameter, α (usually lower than 0.05). The dependent parameter, p_a, represents the abscissa value of the intersection of the cap and shear (or transition) surfaces (Equation 4). Furthermore, the model requires a hardening law of the cap surface determined by the relation of the hydrostatic compression yield stress, p_b, with the volumetric plastic strain, ε_{vol}^{pl}, which can be related to the material density by Equation 5, where ρ_0 is the initial density (loose powder) and ρ is the current density. Finally, within the region limited by the yield surfaces, the material can be modeled with an isotropic linear elastic behavior (defined by Young's modulus, *E*, and Poisson's ratio, ν) [12,18,24,34,35]. The plastic flow potential of the DPC model is implemented in the software ABAQUS using a continuous and smooth plastic potential surface composed of two portions: an associated potential for the cap surface, G_{cap} (identical to the cap yield surface, F_{cap}, in Equation 2) and a nonassociated potential in the shear failure and transition surfaces, G_{shear} (Equation 6) [12,16].

$$F_{shear} = q - ptan\beta - d = 0 \quad \text{(Eq. 1)}$$

$$F_{cap} = \sqrt{(p - p_a)^2 + \left[\frac{Rq}{1+\alpha-\alpha/cos\beta}\right]^2} - R(d + p_a tan\beta) = 0 \quad \text{(Eq. 2)}$$

$$F_{tran} = \sqrt{(p - p_a)^2 + [q - (1 - \alpha/cos\beta)(d + p_a tan\beta)]^2} - \alpha(d + p_a tan\beta) = 0 \quad \text{(Eq. 3)}$$

$$p_a = \frac{p_b - Rd}{1 + Rtan\beta} \quad \text{(Eq. 4)}$$

$$-\varepsilon_{vol}^{pl} = ln(\rho/\rho_0) \quad \text{(Eq. 5)}$$

$$G_{shear} = \sqrt{[(p_a - p)tan\beta]^2 + \left[\frac{q}{(1+\alpha-\alpha/cos\beta)}\right]^2} \quad \text{(Eq. 6)}$$

2.2. Alternatives for calibration of the Drucker-Prager/cap model

One of the great challenges of using the DPC constitutive model is the number and complexity of the experiments required to calibrate its parameters. The calibration of the shear failure surface parameters (d and β) requires at least two tests with distinct stress states. Figure 1 displays four alternatives: uniaxial tension (1), pure shear (2), diametral compression (also known as Brazilian disk test or diametral compression) (3), and uniaxial compression (4) [8,9,12,16,24,35]. Due to the fragile nature of compacted powder materials, diametral and uniaxial compression tests are the most common choices [8,36]. Incorrect calibration of the shear failure parameters can lead to unrealistic simulation results, especially during the unloading and ejection of powder compacts [25,29]. Therefore, it is fundamental to correctly identify the dilatancy of the granular material [29], which is characterized by a permanent increase in the volume caused by shear stress, leading to micro-cracks and material unpacking. [12,13,29]. Identifying plastic dilatancy initiation is still a topic that needs more investigation and discussion [8]. When calibrating the DPC model, most researchers adopted the peak stress (fracture stress) to define the onset of plastic deformation [16,18,21,22,37,38], while others adopted the deviation of linearity [8]. However, it is known that the fracture stress is higher than the actual dilatancy stress [29]. Proper identification of dilatancy would require measuring the volumetric strain, which is difficult using conventional extensometers.

Moreover, the calibration of the cap yield surface parameters (R, α, and $p_b\left(\varepsilon_{vol}^{pl}\right)$) also commonly requires two tests at different stress states [24], though some authors obtained good results adopting only one test based on reasonable assumptions concerning the plastic flow [16]. The first test is an incremental isostatic pressing test used to obtain the hardening law $p_b\left(\varepsilon_{vol}^{pl}\right)$ (Test 6 in Figure 1) [2,12,24,39]. A second test with a stress state that lies in the cap surface is necessary to obtain the cap eccentricity R (Test 5 in Figure 1). This stress state can be obtained through complex triaxial tests [2,40] or a closed die compaction test in an instrumented die (an experimental setup that measures the upper and lower punch loads and the radial pressure in the die wall) [9,16,17,19,22,36,41,42]. The instrumented die has the advantage that it can also be used to determine the friction coefficient, μ, between the powder and the die [35,41,42], but it is not available in many laboratories. Finally, it is unnecessary to have a calibration experiment for the cap transition parameter, α, because it is an artificial parameter used only to avoid numerical instabilities. Thus, it can be set to the lowest possible value that does not cause numerical instabilities without significantly impacting the simulation results [43].

The elastic parameters should also be calibrated. The Young's modulus, E, can be easily obtained with conventional uniaxial compressive tests. On the other hand, obtaining material

Poisson's ratio, v, is more complicated due to the greater difficulty in measuring transversal strain. However, it is crucial to obtain its value because Poisson's ratio strongly influences residual stresses during and after sample ejection [44]. Most authors obtained the elastic parameters during the unloading stages of instrumented closed die compaction tests [16,18,34,35].

Furthermore, it has been shown that all previous parameters can be considered dependent on the compacted density [16]. Therefore, if an accurate prediction of density and stress distribution in the compacted part is required throughout all the simulation stages, the calibration tests previously presented should be repeated for several densities, further increasing the number of required experiments [16].

A possible solution to minimize the number of experiments and maximize the information obtained through them is using DIC. Because it can obtain the full-field measure of displacement, DIC can be used to calculate both the vertical and horizontal strains, thus the volumetric strain, allowing to precisely identify Poisson's ratio and the onset of the dilatancy. For instance, Montilha et al. [29] successfully determined the dilatancy stress of a compacted alumina sample by applying DIC to a cyclic uniaxial compression test. Additionally, DIC can obtain local strain, subtracting the artifacts caused by the testing machine compliance, reducing calibration errors. Further, DIC can identify non-homogeneous strain fields and defects in the sample caused by undesired bending [45] or cracks [46], which might be unnoticed otherwise.

3. MATERIALS AND METHODS

3.1. Calibration of the Drucker-Prager shear surface parameters.

The material used in this study was PZT powder (SP-4, Navy I type) with binder as supplied by the Brazilian Navy Research Institute (IPqM). The median particle size was d_{50} = 3.1 µm, the weight loss on ignition was 0.9 % (350 °C for 2 h), and the helium pycnometer density was 8.00 g/cm^3. The bulk density of the loose powder was 2.75 g/cm^3, which was measured volumetrically by pouring and leveling the powder in a graduated cylinder.

To calibrate the shear surface, DIC was applied to identify the dilatancy on uniaxial compression and diametral compression tests, in a similar manner to what the authors reported in previous studies [29,45]. Three specimens were used for each test. For the uniaxial compression tests, two-dimensional image correlation requires planar faces [32]. Thus, parallelepiped specimens were produced using a hardened steel die with a square hole (18.5 x

18.5 mm) cut by electrical discharge machining and steel punches that were ground and polished to improve the flatness and orthogonality of the faces. The uniaxial compression specimens were pre-compacted uniaxially at 60 MPa in this parallelepiped cavity steel die. For the diametral compression tests, three cylindrical disk specimens were pre-compacted uniaxially at 45 MPa in a cylindrical cavity steel die (inner diameter of 41 mm). To reduce the compaction gradients during pre-compaction, the walls of the molds were lubricated with oleic acid and foam pads were used to support the base of the molds during compaction to mimic the effect of a double-action pressing. After uniaxial pre-compaction, all specimens were isostatically pressed at 200 MPa inside vacuum-sealed thin latex elastomers. A random black-and-white speckle pattern was sprayed onto the specimen surfaces to increase the image contrast and improve DIC resolution [24,45,47,48]. To ensure an adequate contrast, the gray-level histograms of the images were analyzed, where the randomization and dynamic range were verified. Figure 2 displays the molds and the pre-compacted specimens. Tables 1 and 2 display the dimensions and mass of the uniaxial and diametral compression test specimens, respectively.

Table 1 – Dimensions and mass of uniaxial compression test samples.

Specimen	Edge mm	Height mm	Mass g
U1	17.95	33.84	57.88
U2	17.97	36.14	61.96
U3	17.94	40.25	68.93

Table 2 – Dimensions and mass of diametral compression test samples.

Specimen	Diameter mm	Thickness mm	Mass g
D1	39.98	6.03	39.77
D2	40.02	5.70	37.76
D3	40.07	6.00	39.75

The experimental setup for uniaxial compression text is displayed in Figure 3. A similar setup was used for the diametral compression test, changing only the location of the cameras. The tests were performed at an electromechanical universal testing system (MTS Exceed Model E44 with 30kN load cell) (Fig. 3, label 1). The upper and lower parts of the specimens were fixed and aligned on the loading plates (Fig. 3, label 2) using epoxy resin. Figure 4 shows the speckled specimens positioned for the tests. The photos were acquired simultaneously using two cameras (Canon EOS 5DS - 8688 x 5792 pixels, 16bits with EF 180mm f/3.5L Macro USM lenses - Fig. 3, label 3), which were used to check if the strains were similar in two faces of the

specimens, validating the assumption of negligible bending load [45]. White LED was used for specimen illumination (Fig. 3, label 4). The cameras and the illumination LEDs were fixed in rigid supports (Fig. 3, label 5), which were leveled and aligned. The cameras were positioned with the aid of the open-source control software digiCamControl on a laptop (Fig. 3, label 6) connected to the cameras, where the images were verified and recorded. The distance between the cameras and the specimen was about 0.6 m, measured from the camera sensor. Finally, the cameras were triggered by the testing machine controller (Fig. 3, label 7) whenever an established load variation (positive or negative) was exceeded, resulting in an acquisition rate between 0.02 and 0.2 frames per second (fps).

In the uniaxial compression test, the cameras were positioned perpendicular to each other, aligned with two lateral faces of the parallelepiped specimens (Figure 5A). In the diametral compression test, the cameras were positioned facing each other, aligned with the flat faces of the disk specimens (Figure 5B). The cameras were focused on the central area of the specimens, where uniform strain fields were expected. For both tests, the physical size of a pixel was about 9 µm (which was calibrated comparing the number of pixels in the image with the dimensions of the specimens).

The first specimen of each type of test was loaded continuously until fracture to obtain the overall behavior of the loading curve and the fracture stress. The second and third tests consisted of four incremental loading-unloading cycles followed by a final loading until the specimen fractured. Cycled tests allow tracking the plastic strain evolution during unloading, which can be used to identify the dilatancy [29]. A smaller load trigger was used in the second and third specimens of both tests to obtain more detailed loading and unloading curves. Table 3 contains the parameters used in the tests.

Table 3 – Parameters of the uniaxial and diametral compression tests.

Test	Crosshead speed [mm/min]	Load variation trigger for each specimen [N]			Preload [N]	Maximum load in each cycle [N]			
		1º	2º	3º		1º	2º	3º	4º
Uniaxial	0.1	70	40	45	20	300	600	1000	1500
Diametral	0.05	20	5	5	10	30	60	90	120

The DIC was processed using Matlab^{TM} with the Correlli 3.0 framework, developed at LMT ENS Paris-Saclay [49]. Also called global DIC, this algorithm aims to obtain the displacement field $\boldsymbol{u}$, globally minimizing the difference of the gray levels between a reference image $\boldsymbol{f}$ and a deformed image $\boldsymbol{g}$ corrected by the measured displacement. The cost function (Equation 7) is used to describe the gray-level conservation law, where N_i is the number of

pixels in the region of interest and $\boldsymbol{x_i}$ is the coordinate vector of the i-th pixel. To guarantee good conditioning of the minimization, the displacement of the i-th pixel, $\boldsymbol{u_i}$, is described by a set of degrees of freedom via finite element (FE) shape functions (Equation 8), where $\boldsymbol{a_j}$ are the sought nodal displacements, $\boldsymbol{\phi_j}(\boldsymbol{x_i})$ are the FE shape functions, and N_j is the number of nodes.

$$\eta^2 = \sum_i^{N_i}[f(\boldsymbol{x_i}) - g(\boldsymbol{x_i} + \boldsymbol{u_i})]^2 \quad \text{(Eq. 7)}$$

$$\boldsymbol{u_i} = \boldsymbol{u}(\boldsymbol{x_i}) = \sum_j^{N_j} \boldsymbol{\phi_j}(\boldsymbol{x_i})\ \boldsymbol{a_j} \quad \text{(Eq. 8)}$$

Before each test, an initial picture was acquired for each camera to calibrate the reference image $\boldsymbol{f}$. The displacement field was calculated using three-node triangular FE shape functions (T3-DIC) [29,46,47]. A mesh of triangular elements (about 100 elements for uniaxial compression tests and 1200 elements for diametral compression tests) was generated in the region of interest in the center of the pictures. Then, the strains were calculated for each element using the nodal displacements obtained by DIC and the triangular FE shape functions. Because no discontinuities in the strain field were detected, the vertical and horizontal strains at each photo were calculated considering the average strain field of the mesh elements in the analyzed area. Plain stress was assumed in the diametral compression test because the disk diameter was more than five times larger than its thickness [36]. Table 4 presents the expressions used for calculating the volumetric strain (ε_{vol}), the nominal stresses (σ_{xx}, σ_{yy} and σ_{zz}), the equivalent pressure (p) and the equivalent von Mises stress (q), where F is the applied force measured by the testing machine, A is the cross-sectional area of the parallelepiped specimens, D and t are the diameter and the thickness of the disk specimens, respectively. These values were calculated for each picture, considering the average strains. In the uniaxial compression test, the horizontal strains (ε_{xx} and ε_{zz}) were assumed equal, while in the diametral compression test, the strain in the direction of the disk thickness (ε_{zz}) was assumed negligible. The deduction of the diametral compression stress equations [50,51] and the p/q ratio [16] can be found in literature.

Table 4 – Expressions for stresses and volumetric strain of the uniaxial and diametral compression tests.

Test	ε_{vol}	σ_{xx}	σ_{yy}	σ_{zz}	p	q
Uniaxial	$\varepsilon_{yy} + 2\varepsilon_{xx}$	0	$\frac{F}{A}$	0	$\frac{-\sigma_{yy}}{3}$	$-\sigma_{yy}$
Diametral	$\varepsilon_{yy} + \varepsilon_{xx}$	$\frac{-2F}{\pi Dt}$	$-3\sigma_{xx}$	0	$\frac{2\sigma_{xx}}{3}$	$\sqrt{13}\sigma_{xx}$

The elastic constants were obtained considering only the first cycle of the uniaxial compression tests U2 and U3. As discussed in the results section, the second, third, and fourth cycles already presented some plastic deformation, modifying the elastic constants. The Young's modulus was obtained from the slope of the linear fit of the vertical stress (σ_{yy}) by vertical strain (ε_{yy}) curves. Similarly, the Poisson's ratio was obtained from the slope of the linear fit of the horizontal strain (ε_{xx}) by vertical strain (ε_{yy}) curves.

The critical dilatancy stress was defined as the Mises stress occurring at the minimum volumetric strain, as any additional load caused volumetric dilation. The dilatancy stress and the fracture stress of all tests were plotted in the *q vs. p* graph. A linear fit of the failure surface was calculated for the dilatancy and the fracture stresses. The shear failure constants (d and β) were obtained as the linear and angular coefficients of the regression, respectively.

3.2. Calibration of the hardening and the cap surface

An incremental hydrostatic compression test was used to calibrate the cap hardening curve. The PZT powder was pressed uniaxially at 10 MPa in a cylindrical cavity steel die (38 mm diameter – sample H1). Immediately after uniaxial pressing, the mass of the disk was measured. The disk was packed inside a vacuum-sealed elastomer and was isostatically pressed at the following pressures: 20, 40, 60, 80, 120, 160, and 200 MPa. After each pressing stage, the specimen was depressurized, unpacked, and its dimensions were measured before the next pressing stage. The density and the equivalent volumetric plastic strain were calculated for each pressure stage. Two additional replicas (H2 and H3) of the experiment were performed, with slight modifications: die cavity of 41 mm diameter, initial uniaxial pressure of 15 MPa and final isostatic pressure of 190 MPa.

The hardening law was adjusted by an exponential fit [21] with a linear term (Equation 9). The inclusion of the linear term avoided numerical problems in the simulation that arise when the hydrostatic compression yield stress (p_b) does not satisfy $p_b > Rd$ (equivalent to $p_a > 0$) at the beginning of the simulation. The linear term $c_3$was fixed in 0.8 to avoid these numerical problems and satisfy $p_b > Rd$ for both dilatancy and fracture simulations.

$$p_b = c_1 e^{\left(c_2\left(-\varepsilon_{vol}^{pl}\right)\right)} + c_3 \qquad \text{(Eq. 9)}$$

The transition parameter, α, was set the lowest recommend value of 0.01, as it has a negligible effect on the simulation results [12,43]. The cap eccentricity, R, and the friction coefficient, μ, were adopted from previous research with alumina powder [24], another ceramic material. Despite being another material, the cap eccentricity and friction coefficient have less influence when the expected stress field is predominantly hydrostatic, as in the proposed validation study. Furthermore, when comparing the available data for other powder materials, the friction coefficient usually varies between 0.1-0.2 for metallic powders [11,20–22,42,52], 0.2-0.3 for ceramic powders (Alumina [3,24,53], Silicon Carbide [54], and zirconia [55]), and up to 0.45-0.48 for pharmaceutical powders (lactose [4] and microcrystalline cellulose [41]). PZT particles, like other ceramic materials, are mechanically hard and stiff (large Young's modulus) and are expected to behave similarly in friction. Usually, larger friction coefficients enhance shear stresses, increasing shear failure (dilatancy and fracture). Therefore, based on previous research with alumina, the upper limit found in ceramics ($\mu = 0.3$) [24] was adopted as the friction coefficient between the PZT powder and the unlubricated metallic core.

3.3. Case study: isostatic pressing of a hollow hemisphere

A case study was carried out to validate the calibrated parameters of the constitutive model. The proposed geometry was a hollow hemisphere of PZT used as the piezoelectric component of an acoustic transducer. This geometry has a low thickness-to-diameter ratio, making it more susceptible to warping and cracking if the density field is not uniform [3]. Therefore, isostatic pressing is the recommended compaction strategy to obtain parts with high and uniform density [56]. The isostatic mold comprised four pieces: a stainless-steel core, a silicone rubber bag with its cover (to seal the mold), both made of RenCast 4644-1/Huntsman - hardness 41 Shore A, and a 3D-printed ABS polymer jacket, which served to hold the mold components together. The mold was designed with a hemispherical cavity with a cylindrical region with 5 mm height in the base to separate the hemispherical region from the mold base, where density gradients usually occur. Figures 6A and 6B display a digital model of the mold with a sectional cut to reveal its interior and dimensions. Figure 6C displays a photo of the components of the mold.

The proposed geometry was well-suited to the validation study for some reasons. First, the geometry and loadings were distinct from what was used during calibration. Second, the stress conditions in this geometry were mainly hydrostatic during compaction, minimizing the effect of cap eccentricity, *R*, which had not been calibrated for PZT powder. Finally, although the compaction was isostatic, the friction of the powder with the metallic core created shear stresses during unloading, validating the shear surface.

The hemisphere was produced by isostatic pressing at 200 MPa using 27.0 g of PZT powder. The mold was manually fed using a vibratory shaker table, thus increasing the density of the powder inside the mold compared to the loose bulk density. As a result, the initial plastic volumetric strain ($-\varepsilon_{vol}^{pl}|_0$) was higher than zero. This parameter of the constitutive model represents the initial hardening of the model and controls the cap surface position at the beginning of the simulation. The initial density of the powder (3.70 g/cm^3) was calculated volumetrically, considering the mold cavity volume (7.3 cm^3), which resulted in an initial plastic volumetric strain of -0.295 calculated according to Equation 5. Two hemispheres had their external profile measured on a Nikon V-20A profile projector using the 10x magnifying lens. The inner diameters of twenty hemispheres were measured using a three-dimensional measuring machine. The densities of seven fragments of the hemispheres were measured by immersion, based on Archimedes' principle. The method was adapted to use isopropyl alcohol instead of water to avoid destroying the compacted samples [57] because the binder supplied with the powder was water-soluble (probably polyvinyl alcohol).

3.4. Finite element model validation

The simulations of the isostatic pressing of the hollow hemisphere were performed in ABAQUS standard solver with unsymmetric matrix storage to account for the possible unsymmetric material stiffness caused by the nonassociated portion of the plastic flow potential of the DPC model [12]. The PZT powder was modeled using the calibrated DPC model. Three simulations were performed: 1) model with the dilatancy parameters **and** initial hardening; 2) model with the dilatancy parameters **without** initial hardening; 3) model with **fracture** parameters and initial hardening. The purposes of the second and third simulations were to evaluate the effect of the initial hardening and the shear parameters, respectively.

The metallic core was modeled as a rigid surface because the ceramic powder would undergo much larger deformation. It was assumed that the silicone rubber bag would not

significantly influence the simulation because the applied loads are mainly isostatic. Due to geometry and loads symmetry, an axisymmetric model was built. It was assumed that the mold would be overfilled with powder, with a 1 mm height column of powder in the feed channel of the mold. The powder mesh was built with 870 CAX4R elements. Contact was defined using the contact pair algorithm with finite-sliding formulation, surface-to-surface discretization, hard contact normal behavior, and Coulomb friction of 0.3. The metallic core was defined as the master surface.

The degrees of freedom of the metallic core were fully constrained. A radial symmetry boundary condition was imposed on the model. The simulation was performed in three subsequent steps: Initial (application of boundary conditions and contact stabilization); Loading (200 MPa pressure gradually applied to the external surface of the powder); and Unloading (99.7% of pressure gradually removed). Total unloading was not possible due to numerical convergence difficulties related to the non-associated plastic flow potential of the shear failure surface of the DPC model. The FE model is displayed in Figure 7. The ABAQUS input file of simulation 1 (dilatancy parameters with initial hardening) is presented in the supplementary material S1. The density field was calculated with the volume of each element (variable field named EVOL in ABAQUS) according to Equation 10, where $EVOL_0$ and EVOL are the element volume in the initial and current increment of the simulation. The calculation was performed through a macro script written in Python language presented in the supplementary material S2.

$$\rho = \rho_0(EVOL_0/EVOL) \quad \text{(Eq. 1)}$$

4. RESULTS AND DISCUSSIONS

4.1. Calibration results

The strain fields obtained by DIC in the uniaxial and diametral tests were uniform, evidencing that the specimens had no discontinuities caused by cracks or undesired bending, validating the initial assumption of uniform strain in the calculations. Furthermore, discontinuities caused by crack initiation were observed only near the end of the tests when the specimens fractured (as expected).

The uniaxial compression test stress-strain curve is presented in Figure 8. The incremental load cycles evidenced the progressive plastic deformation. As previously discussed, the elastic parameters were obtained considering only the first cycle. It can be

observed in Figure 8 that only the first cycle presented negligible plastic deformation, fully recovering the deformation. The calibrated elastic parameters are presented in Table 5.

The presence of significant plastic deformation in final cycles was an indicator that dilatancy had already taken place. To better visualize the effect of dilatancy, a graph of the deviatoric strain by volumetric strain in the uniaxial test is presented in Figure 9. During the initial stages of the test, the volumetric strain decreased (specimen volume reduced). However, as compaction continued, the volumetric strain reverted its decreasing tendency and started to increase. The volumetric strain significantly increased during the final cycle, exceeding the initial volume reduction and becoming positive (specimen volume increased). The dilatancy point was defined at the minimum volumetric strain (when the material started to expand due to the increasing load). The dilatancy stress was obtained from the equivalent Mises stress at this point.

Table 5 – PZT elastic parameters obtained in the uniaxial compression test and the respective coefficients of determination of the linear regressions.

Specimen	Camera	E GPa	R^2 -	ν -	R^2 -
U2	1	1.70	0.96	0.180	0.96
U2	2	1.55	0.95	0.173	0.80
U3	1	1.81	0.94	0.195	0.75
U3	2	1.88	0.95	0.164	0.69
Average		**1.8**		**0.18**	
Std deviation		**0.1**		**0.01**	

Concerning the diametral compression test, a similar analysis was made. The vertical stress-strain curve of a diametral test is presented in Figure 10. The dilatancy point was identified in the deviatoric strain by the volumetric strain graph in Figure 11. In contrast to the uniaxial results, performing a cycled test of the diametral compression added no relevant information and made the analysis more difficult due to the larger number of points. For future studies, monotonical loading is recommended instead of cycled loading-unloading for the diametral test. Furthermore, diametral tests also presented more noise and larger deviation, highlighting the importance of using more than one sample.

The dilatancy stress and the fracture stresses for the three uniaxial compression tests are summarized in Table 6. The Drucker-Prager shear surfaces were obtained through a linear fit of the stresses of uniaxial and diametral compression tests. Figure 12 depicts the results in the *p-q* plane considering both dilatancy and fracture.

Table 6– Dilatancy and fracture stresses at the uniaxial and diametral compression tests.

Specimen	Dilatancy	Fracture

	MPa	MPa
U1	2.431	6.104
U2	2.401	6.765
U3	2.849	6.729
D1	0.918	2.029
D2	1.200	2.351
D3	0.806	1.630

It can be observed that the dilatancy stress is much smaller than the fracture stress. Thus, when the material is subjected to shear, unpacking and crack initiation occur before fracturing [29]. Consequently, using the dilatancy stress instead of fracture stress is more indicated when modeling compacted powder shear failure.

The hydrostatic compression test results and the exponential fit obtained for the cap hardening are presented in Figure 13. The constants of the exponential fit (Equation 9) were calculated as c_1 = 6.31·10^{-4} MPa, c_2 = 21.2, and c_3 = 0.8 MPa, with R^2 of 97.1%. Table 7 summarizes all parameters of the Drucker-Prager/cap model used in the simulations. The parameter *K* is the yield stress ratio in triaxial tension to triaxial compression, and it is usually assumed as one [12]. Although no data about PZT Drucker-Prager/cap parameters were found in literature, the parameters obtained in this study were in a similar range to other powder materials (Table 8), evidencing a reasonable behavior.

Table 7 –Drucker-Prager/cap parameters for PZT in the simulations.

Simulation	E	ν	d	B	R	$-\varepsilon_{vol}^{pl}\|_0$	α	K
	GPa	-	MPa	Degrees	-	-	-	-
1 – dilatancy with initial hardening	1.758	0.178	0.537	67.21	0.75	0.295	0.01	1
2 – dilatancy without initial hardening	1.758	0.178	0.537	67.21	0.75	**0**	0.01	1
3 – fracture with initial hardening	1.758	0.178	**1.06**	**68.31**	0.75	0.295	0.01	1

Table 8 –Drucker-Prager/cap parameters and friction coefficient between powder materials and die walls obtained from literature (for comparison).

Material	E	v	d	β	R	α	μ	Reference
	GPa	-	MPa	Degrees	-	-	-	
Microcrystalline cellulose (60% density)	1.0	0.2	1.0	72	0.6	0	0.26	[17]
Graphite	-	-	1.0	60	0.7	0	-	[8]
LiNiMnCoO2 (NMC)	-	-	4.0	65	0.8	0	-	[8]
Alumina	2.7	0.13	3.25	55	0.75	0	0.3	[24]

4.2. Validation results

Figure 14 displays two compacted hemispheres. The pressed parts had an average external diameter of 32.4 ± 0.1 mm and an inner diameter of 26.48 ± 0.01 mm. Supplementary material S3 includes the measured profiles data. In contrast, in the simulation with dilatancy and initial hardening (Simulation 1), the part had an external diameter of 32.53 mm and an inner diameter of 26.78 mm, 0.4% and 1.1% larger than the measured dimensions, respectively. The dimensions were evaluated 5 mm above the base of the part (the junction between the hemispherical and cylindrical regions). The average density of the pressed parts was 5.09 ± 0.02 g/cm^3 (63.5% of the theoretical maximum). In contrast, the simulated part density varied from 5.05 to 4.92 in the hemispherical region (the average was 4.99 g/cm^3, 2.0% smaller than measured). The comparison of the measured and simulated cross-section profiles is depicted in Figure 15Figure 15, which also presents the simulated density field.

The simulated profile presented high similarity with the pressed part, visually and numerically. Both the measured and simulated inner diameters were slightly larger than the mold core diameter (26.36 mm). The gap between the metallic core and the part is displayed in Figure 16A. The elastic springback of the part caused this gap during unloading. The simulation predicted the springback accurately, pointing out that the calibration of the elastic parameters was validated. Even though the model partially included powder data from other ceramic material (alumina) (R and μ), the FE simulation accurately modeled the compaction process, validating the calibration procedures.

The differences in the results should also be highlighted. The measured part presented a thickness reduction from bottom to top. It can be observed in Figure 15 that the measured profile in the bottom was similar to the simulation with initial hardening (Simulation 1). On the other hand, the simulation without hardening (Simulation 2) better represented the compaction behavior in the upper region of the part. As a result of the mold filling process, the powder in the bottom was more tapped than the powder at the top. Consequently, the powder at the bottom had a larger initial density and suffered less volumetric compaction than the upper region, resulting in a thicker wall.

Furthermore, a defect known as “elephant foot” [58] was observed in the base of the part (Figure 16). This defect was caused by the friction of the powder with the mold base (which was intensified by the limited deformation of the rubber in the edge of the metallic core, as observed in the projected profile in Figure 16B). Consequently, the bottom of the part presented a less dense region with an intense density gradient, as observed in Figure 16A. Furthermore,

the similar shape of the bottom indicates that the assumption of μ = 0.3 is close to the actual friction coefficient of PZT powder.

Finally, Figure 17 compares the simulations with the fracture and dilatancy calibrated parameters. As can be observed, adopting the fracture data led to underestimating the regions where there was plastic volumetric expansion and damage initiation. Conversely, adopting the dilatancy data calibrated using DIC allowed more accurate identification of regions susceptible to failures. In the proposed geometry, the bottom edge and some external surface areas were the regions with dilatancy, smaller density, and more intense density gradient than the rest of the part. These regions may cause significant defects because density gradients greater than 1%/mm can introduce cracks or considerable warping during sintering [3]. For this geometry, green machining should be used to correct the non-uniform thickness of the part and to remove the damaged regions before sintering, improving the mechanical properties of the final part [3]. Therefore, the accurate identification of the critical regions is fundamental for planning the amount of material that should be removed during the green machine step. The proposed methodology for calibration of the DPC model using DIC allowed better identification of the onset of dilatancy, resulting in a more accurate simulation than what could be achieved using other calibration strategies.

5. CONCLUSIONS

The finite element (FE) simulation with the adjusted Drucker-Prager/cap (DPC) parameters allowed a deeper understanding of the pressing process, predicting the shape, dimensions, and density field of the pressed part. The design of molds can be notably aided by numerical simulation, as it reduces trial-and-error, saving time and resources. The use of digital image correlation (DIC) allowed obtaining more information from the uniaxial and diametral compression tests, including the Poison's ratio. Remarkably, because DIC is a full-field strain measurement, the proposed methodology was able to identify the onset of dilatancy, which occurs in lower stress than fracture, and may not be obtained with traditional calibration techniques. Therefore, the shear failure surface parameters of the DPC model were calibrated with improved accuracy. With the additional information obtained by DIC, only three types of simple tests (uniaxial compression, diametral compression, and volumetric compression) resulted in a near-complete calibration of the DPC model, without complex triaxial tests or instrumented dies. Despite no calibration of the cap eccentricity, R, and friction coefficient, μ, the numerical validation showed significant agreement with the experimental measures with a

difference of only 1.2% in the internal diameter and 2.2% in the density, highlighting the success of DIC to obtain accurate results, especially for near isostatic pressing. The method proved to be an efficient tool for predicting critical regions susceptible to deformation and cracking during the sintering shrinkage, allowing better planning of the green machining step. The proposed methodology can be used to calibrate other powder materials in which dilatancy plays a key role. In future developments, the constitutive model of the powder calibrated in this work has a potential application in the design of molds for other PZT components with dimensions or geometries different from those used in this paper.

Some concerns about the limitations of the present study and possible alternatives should be noted. In this paper, the DPC model was considered density-independent. If a density-dependent model had been chosen, the parameters should have been calibrated at several density values [16,35,38,59]. Nevertheless, the DIC methodology could be easily extended to calibrate a series of uniaxial and diametral compression tests with specimens with incremental densities. The full-field measure could also be used to calibrate non-linear elastic parameters, implementing more complex DPC models such as proposed by Han et al. [16]. Furthermore, despite the excellent validation results, the calibrated parameters did not include the R and μ. There are two possible alternatives that do not require instrumented die nor triaxial tests. First, ZHU et al. [8] used DIC to perform closed die compaction and measure the radial and axial deformation of the die, thus obtaining similar results to an instrumented die. This alternative takes advantage of the DIC equipment used to calibrate the shear failure surface, allowing full calibration of the DPC model. The second alternative is to combine the DIC calibration with inverse analysis optimization to obtain the missing parameters [24]. The DIC calibration has the advantage of reducing the number of parameters required for the inverse analysis, improving its accuracy, and reducing its computational cost.

CRediT AUTHOR STATEMENT

Mateus Morais: Experimental investigation, Numerical analysis, Writing – original draft preparation. Caiuã Melo: Experimental investigation, Software – supporting algorithms, Writing – reviewing and editing. Rodrigo Canto: Conceptualization, Writing – reviewing and editing, Funding acquisition. Carlos Fortulan: Writing – reviewing and editing, Supervision, Funding acquisition.

ACKNOWLEDGEMENTS

This study was financed by the Coordenação de Aperfeiçoamento de Pessoal de Nível Superior – Brasil (CAPES) – Finance Code 001, the São Paulo Research Foundation (FAPESP) [grants 2018/07928-2 and 2018/02801-4], and the National Council for Technological and Scientific Development (CNPq) [grants 131685/2018-0 and 309422/2019-1]. We acknowledge the collaboration of Professor Renato Goulart Jasinevicius that made available the profile projector and of IPqM (Brazilian Navy Research Institute) that provided the PZT powder.

DECLARATION OF COMPETING INTEREST

The authors declare that they have no known competing financial interests or personal relationships that could have appeared to influence the work reported in this paper.

REFERENCES

[1] A.C.F. Cocks, I.C. Sinka, Constitutive modelling of powder compaction - I. Theoretical concepts, Mech. Mater. 39 (2007) 392–403. https://doi.org/10.1016/j.mechmat.2006.09.003.

[2] H. Chtourou, M. Guillot, A. Gakwaya, Modeling of the metal powder compaction process using the cap model. Part I. Experimental material characterization and validation, Int. J. Solids Struct. 39 (2002) 1059–1075. https://doi.org/10.1016/S0020-7683(01)00255-4.

[3] H. Zipse, Finite-element simulation of the die pressing and sintering of a ceramic component, J. Eur. Ceram. Soc. 17 (1997) 1707–1713. https://doi.org/10.1016/S0955-2219(97)00037-X.

[4] C.Y. Wu, O.M. Ruddy, A.C. Bentham, B.C. Hancock, S.M. Best, J.A. Elliott, Modelling the mechanical behaviour of pharmaceutical powders during compaction, Powder Technol. 152 (2005) 107–117. https://doi.org/10.1016/j.powtec.2005.01.010.

[5] İ. Aydin, B.J. Briscoe, K.Y. Şanlitürk, The internal form of compacted ceramic components: a comparison of a finite element modelling with experiment, Powder Technol. 89 (1996) 239–254. https://doi.org/10.1016/S0032-5910(96)03188-9.

[6] I.C. Sinka, J.C. Cunningham, A. Zavaliangos, Analysis of tablet compaction. II. Finite element analysis of density distributions in convex tablets, J. Pharm. Sci. 93 (2004) 2040–2053. https://doi.org/10.1002/jps.20111.

[7] C.Y. Wu, B.C. Hancock, A. Mills, A.C. Bentham, S.M. Best, J.A. Elliott, Numerical

and experimental investigation of capping mechanisms during pharmaceutical tablet compaction, Powder Technol. 181 (2008) 121–129. https://doi.org/10.1016/j.powtec.2006.12.017.

[8] J. Zhu, W. Li, T. Wierzbicki, Y. Xia, J. Harding, Deformation and failure of lithium-ion batteries treated as a discrete layered structure, Int. J. Plast. 121 (2019) 293–311. https://doi.org/10.1016/j.ijplas.2019.06.011.

[9] I.C. Sinka, Modelling Powder Compaction, KONA Powder Part. J. 25 (2007) 4–22. https://doi.org/10.14356/kona.2007005.

[10] J. Cunningham, K. LaMarche, A. Zavaliangos, Modeling of powder compaction with the drucker–prager cap model, in: Predict. Model. Pharm. Unit Oper., Elsevier, 2017: pp. 205–227. https://doi.org/10.1016/B978-0-08-100154-7.00008-9.

[11] A. Atrian, G.H. Majzoobi, B. Markert, S.H. Nourbakhsh, A novel approach to calibrate the Drucker–Prager Cap model for Al7075 powder, Arch. Appl. Mech. 88 (2018) 1859–1876. https://doi.org/10.1007/s00419-018-1410-x.

[12] Dassault Systèmes, Abaqus 6.14 Online Documentation - Abaqus Analysis User's Guide, 2014.

[13] D.C. Drucker, W. Prager, Soil mechanics and plastic analysis or limit design, Q. Appl. Math. 10 (1952) 157–165. https://doi.org/10.1090/qam/48291.

[14] E. Papamichos, Analytical models for onset of sand production under isotropic and anisotropic stresses in laboratory tests, Geomech. Energy Environ. 21 (2020) 100149. https://doi.org/10.1016/j.gete.2019.100149.

[15] W. Jin, J.L. Klinger, T.L. Westover, H. Huang, A density dependent Drucker-Prager/Cap model for ring shear simulation of ground loblolly pine, Powder Technol. 368 (2020) 45–58. https://doi.org/10.1016/j.powtec.2020.04.038.

[16] L.H. Han, J.A. Elliott, A.C. Bentham, A. Mills, G.E. Amidon, B.C. Hancock, A modified Drucker-Prager Cap model for die compaction simulation of pharmaceutical powders, Int. J. Solids Struct. 45 (2008) 3088–3106. https://doi.org/10.1016/j.ijsolstr.2008.01.024.

[17] S. Ohsaki, K. Kushida, Y. Matsuda, H. Nakamura, S. Watano, Numerical study for tableting process in consideration of compression speed, Int. J. Pharm. 575 (2020) 118936. https://doi.org/10.1016/j.ijpharm.2019.118936.

[18] H. Diarra, V. Mazel, A. Boillon, L. Rehault, V. Busignies, S. Bureau, P. Tchoreloff, Finite Element Method (FEM) modeling of the powder compaction of cosmetic products: Comparison between simulated and experimental results, Powder Technol. 224 (2012) 233–240. https://doi.org/10.1016/j.powtec.2012.02.058.

[19] F. Zou, S. Huang, M. Zhou, Y. Lei, S. Yan, J. Zhang, B. Wang, Constitutive model and compaction equation for aluminum alloy powder during compaction, J. Adv. Mech. Des. Syst. Manuf. 13 (2019) 1–13. https://doi.org/10.1299/jamdsm.2019jamdsm0015.

[20] S.M. Wang, Y. Wang, Y.X. Wang, F.P. Liu, J. Cao, Stresses State and Mechanical Behaviors of the Green Body During Die Compaction and Ejection Process, Acta Metall. Sin. (English Lett. 33 (2020) 605–614. https://doi.org/10.1007/s40195-020-01018-y.

[21] M.T. Hasan, C. Li, Y. Shen, A. Yu, R. Yang, Finite element analysis of briquetting of iron ore fines, Powder Technol. 353 (2019) 398–408. https://doi.org/10.1016/j.powtec.2019.05.026.

[22] M. Zhou, S. Huang, Y. Lei, W. Liu, S. Yan, Investigation on Compaction Densification Behaviors of Multicomponent Mixed Metal Powders to Manufacture Silver-Based Filler Metal Sheets, Arab. J. Sci. Eng. 44 (2019) 1321–1335. https://doi.org/10.1007/s13369-018-3505-7.

[23] H. Staf, E. Olsson, P.-L. Larsson, Mechanical characterization of powder materials: A general approach detailed for cemented carbides, Powder Technol. 364 (2020) 531–537. https://doi.org/10.1016/j.powtec.2020.02.025.

[24] C.C. Melo, A.L.I. Moraes, F.O. Rocco, F.S. Montilha, R.B. Canto, A validation procedure for numerical models of ceramic powder pressing, J. Eur. Ceram. Soc. 38 (2018) 2928–2936. https://doi.org/10.1016/j.jeurceramsoc.2018.01.009.

[25] T. Sinha, J.S. Curtis, B.C. Hancock, C. Wassgren, A study on the sensitivity of Drucker-Prager Cap model parameters during the decompression phase of powder compaction simulations, Powder Technol. 198 (2010) 315–324. https://doi.org/10.1016/j.powtec.2009.10.025.

[26] R. Zhou, L. Yang, Z. Liu, B. Liu, Modeling the powder compaction process by an integrated simulation and inverse optimization method, Mater. Today Commun. 25 (2020) 101475. https://doi.org/10.1016/j.mtcomm.2020.101475.

[27] S. Pandey, V. Buljak, I. Balac, Reduced order numerical modeling for calibration of complex constitutive models in powder pressing simulations, Sci. Sinter. 49 (2017) 331–345. https://doi.org/10.2298/SOS1703331P.

[28] G.H. Majzoobi, S. Jannesari, Determination of the constants of cap model for compaction of three metal powders, Adv. Powder Technol. 26 (2015) 928–934. https://doi.org/10.1016/j.apt.2015.03.008.

[29] F.S. Montilha, F.O. Rocco, C.C. Melo, V.F. Sciuti, R.B. Canto, Identification of dilatancy in green compacted ceramic powder via digital image correlation, Powder Technol. 330 (2018) 471–476. https://doi.org/10.1016/j.powtec.2018.01.037.

[30] H. Leclerc, J.-N. Périé, S. Roux, F. Hild, Integrated Digital Image Correlation for the Identification of Mechanical Properties, in: Lect. Notes Comput. Sci. (Including Subser. Lect. Notes Artif. Intell. Lect. Notes Bioinformatics), 2009: pp. 161–171. https://doi.org/10.1007/978-3-642-01811-4_15.

[31] F. Hild, S. Roux, Digital image correlation: From displacement measurement to identification of elastic properties - A review, Strain. 42 (2006) 69–80. https://doi.org/10.1111/j.1475-1305.2006.00258.x.

[32] B. Pan, Digital image correlation for surface deformation measurement: Historical developments, recent advances and future goals, Meas. Sci. Technol. 29 (2018). https://doi.org/10.1088/1361-6501/aac55b.

[33] S. Shima, K. Mimura, Densification behaviour of ceramic powder, Int. J. Mech. Sci. 28 (1986) 53–59. https://doi.org/10.1016/0020-7403(86)90007-X.

[34] C. Shang, I.C. Sinka, J. Pan, Constitutive Model Calibration for Powder Compaction Using Instrumented Die Testing, Exp. Mech. 52 (2012) 903–916. https://doi.org/10.1007/s11340-011-9542-8.

[35] J.C. Cunningham, I.C. Sinka, A. Zavaliangos, Analysis of tablet compaction. I. Characterization of mechanical behavior of powder and powder/tooling friction, J. Pharm. Sci. 93 (2004) 2022–2039. https://doi.org/10.1002/jps.20110.

[36] P. Doremus, F. Toussaint, O. Alvain, Simple Tests and Standard Procedure for the Characterisation of Green Compacted Powder, in: A. Zavaliangos, A. Laptev (Eds.), Recent Dev. Comput. Model. Powder Metall. Process., IOS Press, Amsterdam, 2001: pp. 29–41.

[37] S. Garner, J. Strong, A. Zavaliangos, The extrapolation of the Drucker–Prager/Cap material parameters to low and high relative densities, Powder Technol. 283 (2015) 210–226. https://doi.org/10.1016/j.powtec.2015.05.027.

[38] M. Zhou, S. Huang, J. Hu, Y. Lei, Y. Xiao, B. Li, S. Yan, F. Zou, A density-dependent modified Drucker-Prager Cap model for die compaction of Ag57.6-Cu22.4-Sn10-In10 mixed metal powders, Powder Technol. 305 (2017) 183–196. https://doi.org/10.1016/j.powtec.2016.09.061.

[39] W. He, Q. Wei, K. Liu, Y. Shi, J. Liu, Numerical simulation of cold isostatic pressed alumina parts produced by selective laser sintering and part shape optimization, Ceram. Int. 39 (2013) 9683–9690. https://doi.org/10.1016/j.ceramint.2013.04.086.

[40] H. Park, K.T. Kim, Consolidation behavior of SiC powder under cold compaction, Mater. Sci. Eng. A. 299 (2001) 116–124. https://doi.org/10.1016/S0921-5093(00)01419-2.

[41] I.C. Sinka, J.C. Cunningham, A. Zavaliangos, The effect of wall friction in the compaction of pharmaceutical tablets with curved faces: A validation study of the Drucker-Prager Cap model, Powder Technol. 133 (2003) 33–43. https://doi.org/10.1016/S0032-5910(03)00094-9.

[42] H. Staf, P.L. Larsson, Evaluation of an advanced powder-die frictional model, Powder Technol. 363 (2020) 569–574. https://doi.org/10.1016/j.powtec.2020.01.048.

[43] H. Shin, J.-B. Kim, Physical interpretations for cap parameters of the modified Drucker-Prager cap model in relation to the deviator stress curve of a particulate compact in conventional triaxial testing, Powder Technol. 280 (2015) 94–102. https://doi.org/10.1016/j.powtec.2015.04.023.

[44] H. Diarra, V. Mazel, V. Busignies, P. Tchoreloff, Sensitivity of elastic parameters during the numerical simulation of pharmaceutical die compaction process with Drucker-Prager/Cap model, Powder Technol. 332 (2018) 150–157. https://doi.org/10.1016/j.powtec.2018.03.068.

[45] C.C. de Melo, M. Furlan, F. Hild, N. Schmitt, R.B. Canto, Uniaxial compression test on ceramic green compact with bending consideration using digital image correlation, Powder Technol. 376 (2020) 136–148. https://doi.org/10.1016/j.powtec.2020.08.002.

[46] R. Vargas, J. Neggers, R.B. Canto, J.A. Rodrigues, F. Hild, Comparison of two full-

field identification methods for the wedge splitting test on a refractory, J. Eur. Ceram. Soc. 38 (2018) 5569–5579. https://doi.org/10.1016/j.jeurceramsoc.2018.07.039.

[47] G. Besnard, F. Hild, S. Roux, "Finite-Element" Displacement Fields Analysis from Digital Images: Application to Portevin–Le Châtelier Bands, Exp. Mech. 46 (2006) 789–803. https://doi.org/10.1007/s11340-006-9824-8.

[48] B. Pan, K. Qian, H. Xie, A. Asundi, Two-dimensional digital image correlation for in-plane displacement and strain measurement: A review, Meas. Sci. Technol. 20 (2009). https://doi.org/10.1088/0957-0233/20/6/062001.

[49] H. Leclerc, J. Neggers, F. Mathieu, F. Hild, S. Roux, Correli 3.0, IDDN. FR. 001.520008. 000. SP 2015.000. 31500, (2015).

[50] M.K. Fahad, Stresses and failure in the diametral compression test, J. Mater. Sci. 31 (1996) 3723–3729. https://doi.org/10.1007/BF00352786.

[51] D.C. Cranmer, D.W. Richerson, Mechanical Testing Methodology for Ceramic Design and Reliability, CRC Press, Boca Raton, FL, 1998.

[52] H. Staf, E. Olsson, P. Lindskog, P.-L. Larsson, Determination of the Frictional Behavior at Compaction of Powder Materials Consisting of Spray-Dried Granules, J. Mater. Eng. Perform. 27 (2018) 1308–1317. https://doi.org/10.1007/s11665-018-3205-1.

[53] B.J. Briscoe, P.D. Evans, Wall friction in the compaction of agglomerated ceramic powders, Powder Technol. 65 (1991) 7–20. https://doi.org/10.1016/0032-5910(91)80165-F.

[54] M. Reiterer, T. Kraft, U. Janosovits, H. Riedel, Finite element simulation of cold isostatic pressing and sintering of SiC components, Ceram. Int. 30 (2004) 177–183. https://doi.org/10.1016/S0272-8842(03)00086-5.

[55] K.T. Kim, S.W. Choi, H. Park, Densification Behavior of Ceramic Powder Under Cold Compaction, J. Eng. Mater. Technol. 122 (2000) 238–244. https://doi.org/10.1115/1.482793.

[56] D.W. Richerson, Modern ceramic engineering: properties, processing, and use in design, 3rd ed., CRC Press, Boca Raton, 2005.

[57] J. Ito, Y. Matsushima, H. Unuma, N. Horiuchi, K. Yamashita, M. Tajika, Preparation

and properties of pressureless-sintered dense calcite ceramics, Mater. Chem. Phys. 192 (2017) 304–310. https://doi.org/10.1016/j.matchemphys.2017.01.062.

[58] M. Koizumi, M. Nishihara, eds., Isostatic pressing: technology and applications, Elsevier Science Publisher Ltd, New York, 1991.

[59] H. Diarra, V. Mazel, V. Busignies, P. Tchoreloff, Comparative study between Drucker-Prager/Cap and modified Cam-Clay models for the numerical simulation of die compaction of pharmaceutical powders, Powder Technol. 320 (2017) 530–539. https://doi.org/10.1016/j.powtec.2017.07.077.

FIGURES

Figure 1 – Drucker-Prager/*cap* model and possible tests to calibrate the yield curves. Adapted from [9,12,16].

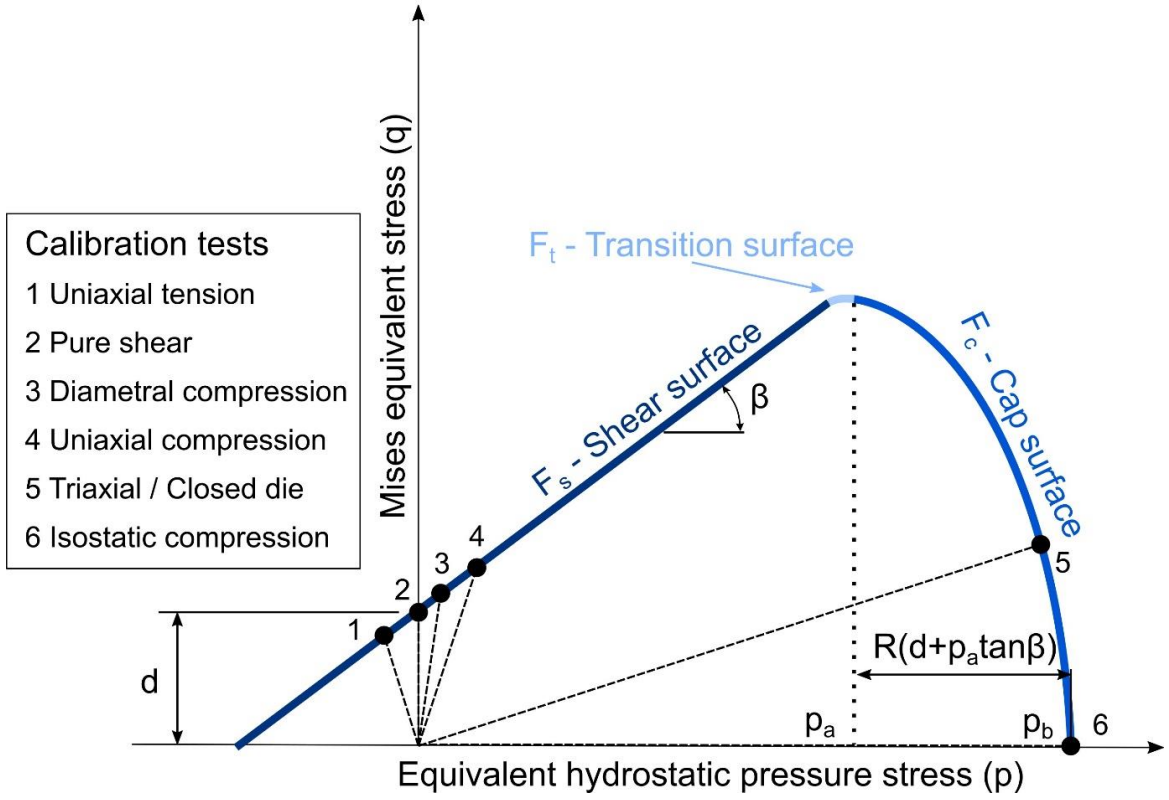

Figure 2 – Photos of molds and pre-compacted specimens. A) Samples for uniaxial compression. B) Samples for diametral compression

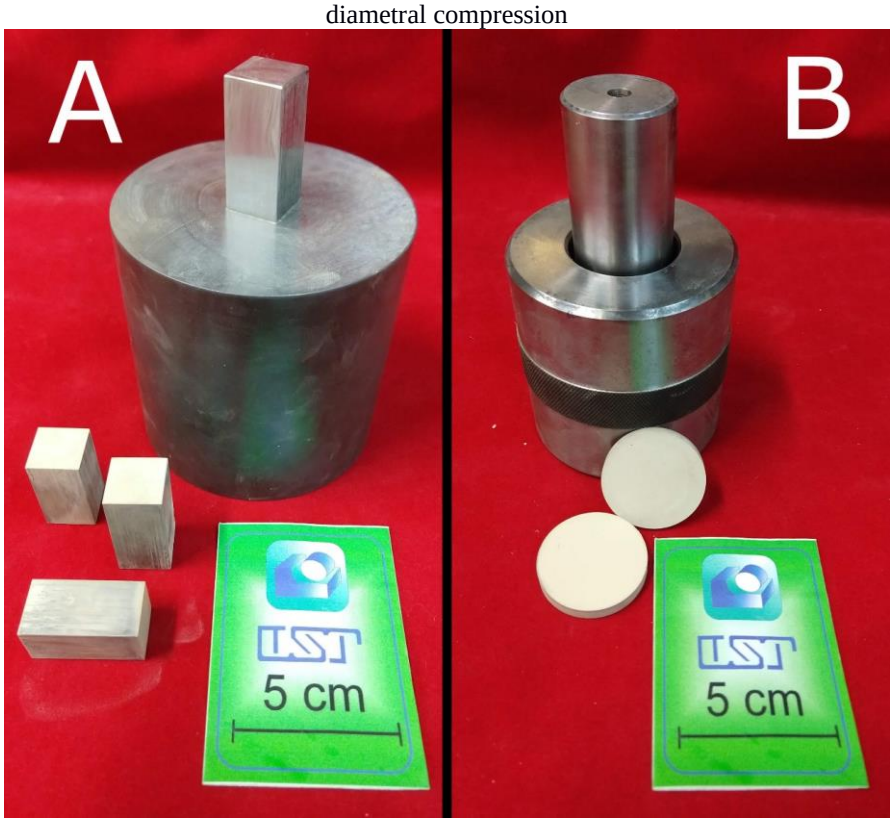

Figure 3 – Photos of the experimental setup for the uniaxial compression test. In A, frontal view. In B, lateral view. Legend: 1 – Universal testing machine; 2 – Loading plates; 3 – Digital cameras with Macro lens; 4 – LED lights; 5 – Leveled rigid supports; 6 – Laptop with software for controlling the cameras; 7 – Computer with the test machine controller.

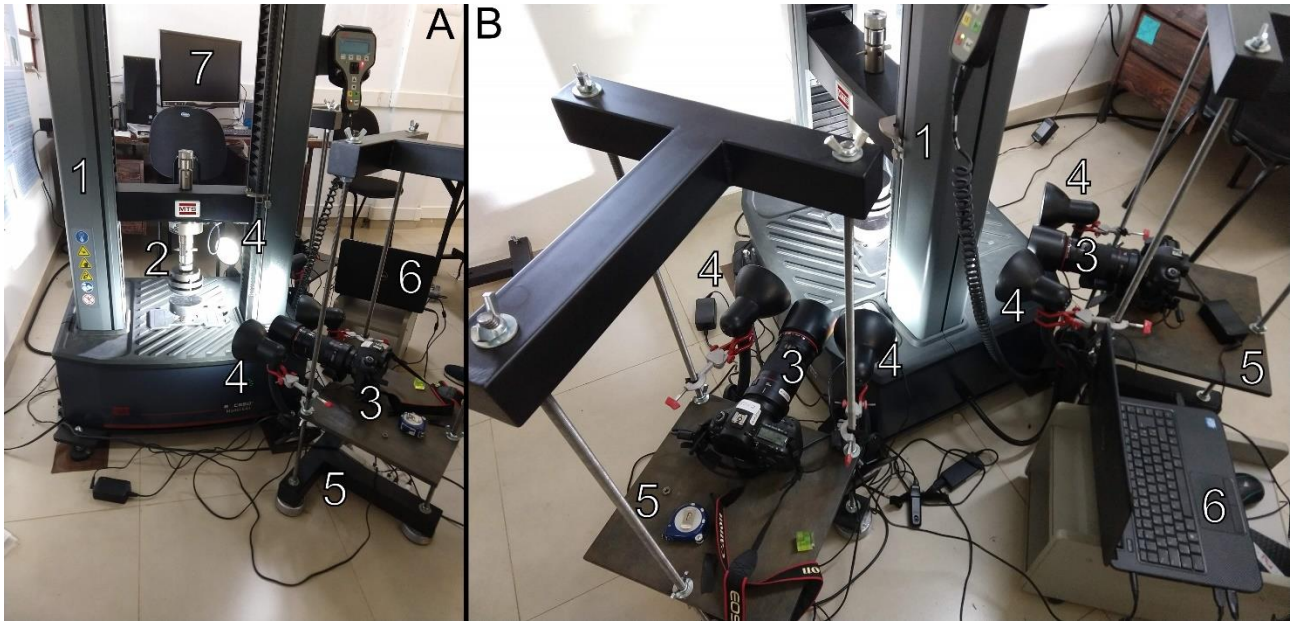

Figure 4 – Specimens with random speckle pattern positioned on the testing machine. A) Uniaxial compression specimen. B) A Diametral compression specimen.

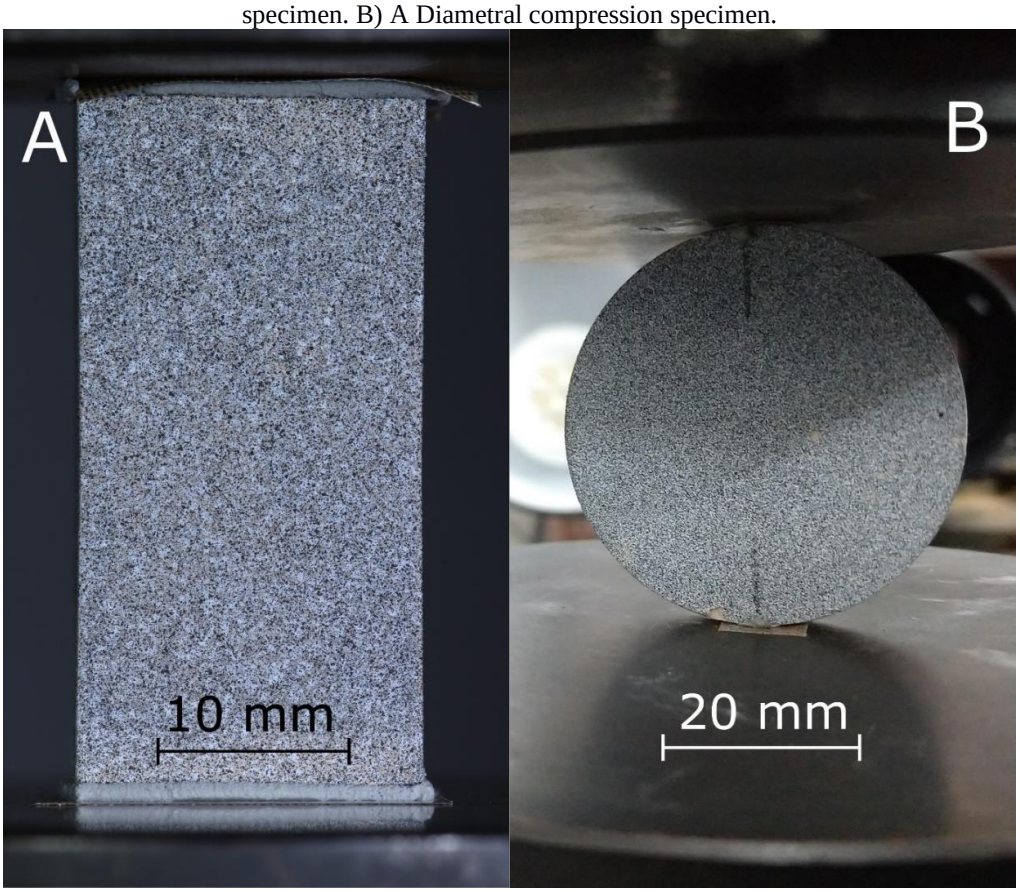

Figure 5 – Illustration of the arrangement of the cameras. A) Uniaxial compression test (90° angle). B) Diametral compression test (180° angle).

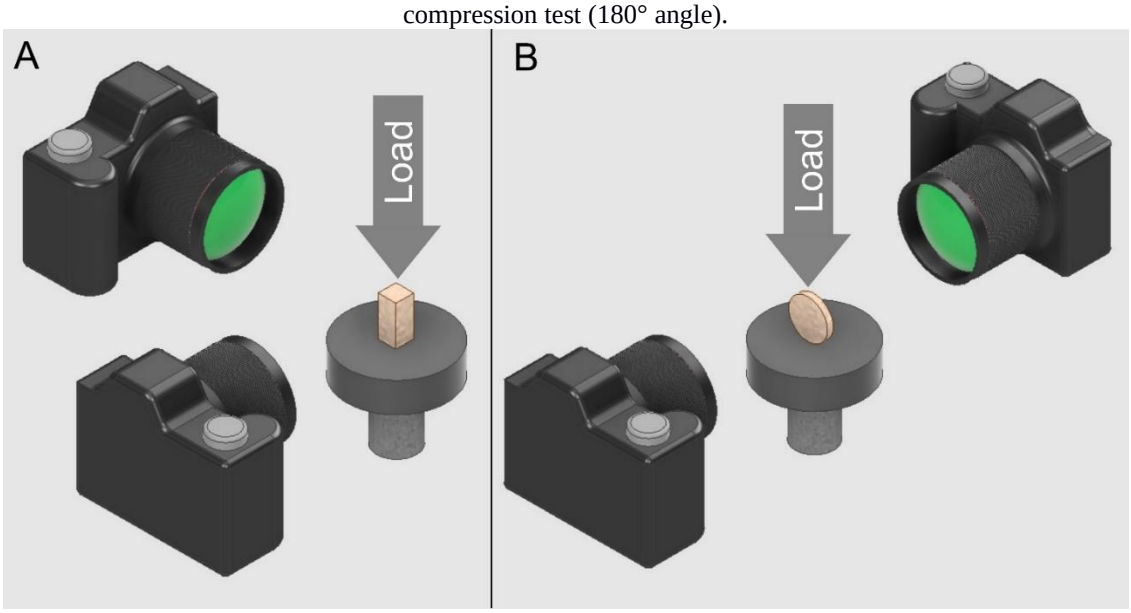

Figure 6 – Isostatic mold. A – Perspective view of a digital representation of the mold with section cut (the colors are only illustrative). B – Main dimensions of the mold. Dimensions in millimeters. C – Picture of the mold components and a pressed hemisphere.

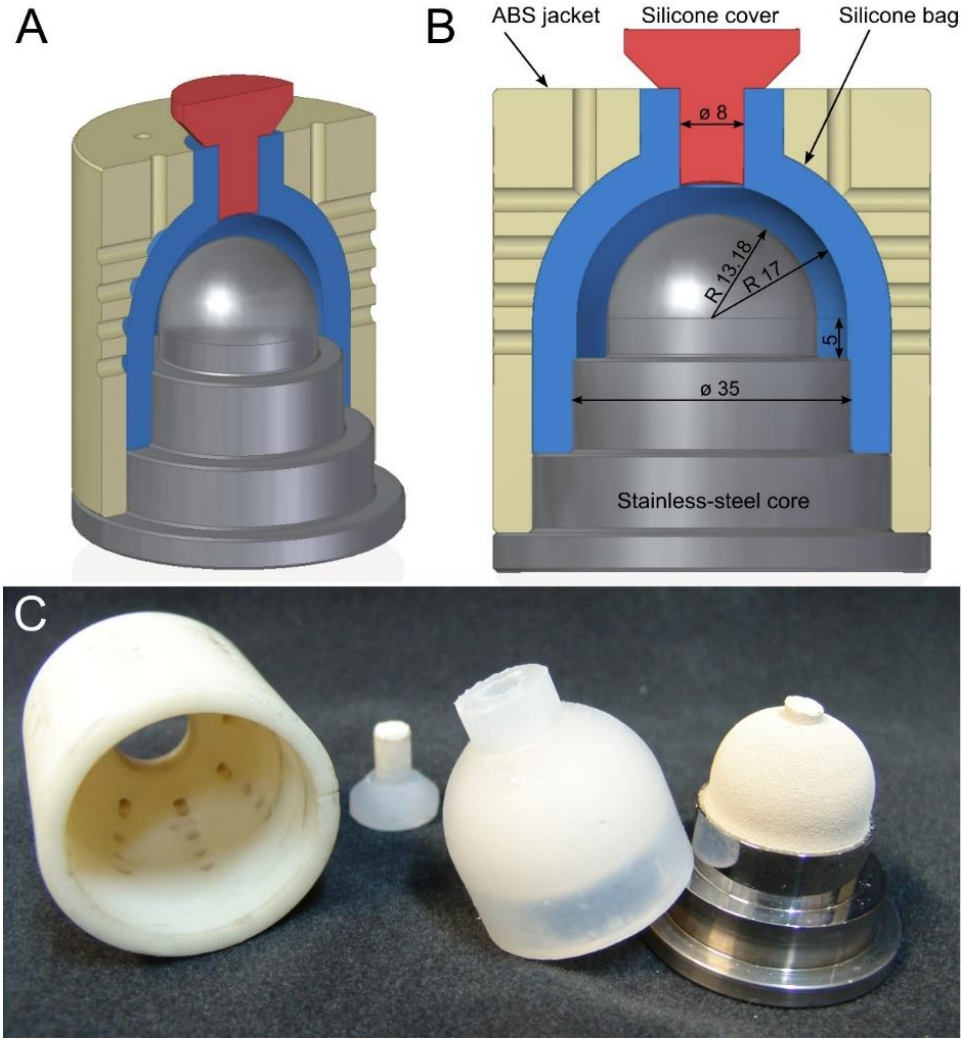

Figure 7 – Axisymmetric section of the FE model. Representation of the powder mesh with the main dimensions and with the loadings. Dimensions in millimeters. Symmetry axis on the left.

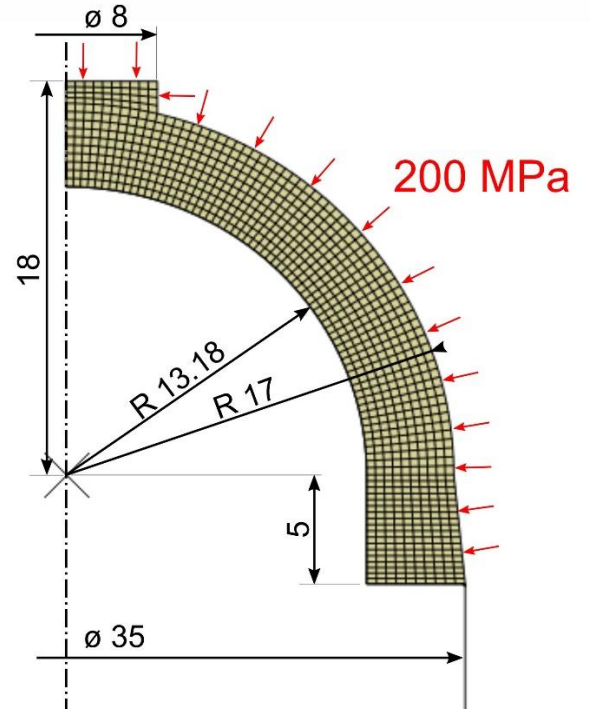

Figure 8 – Cycled uniaxial compression test of specimen U3. The first cycle presents negligible plastic deformation.

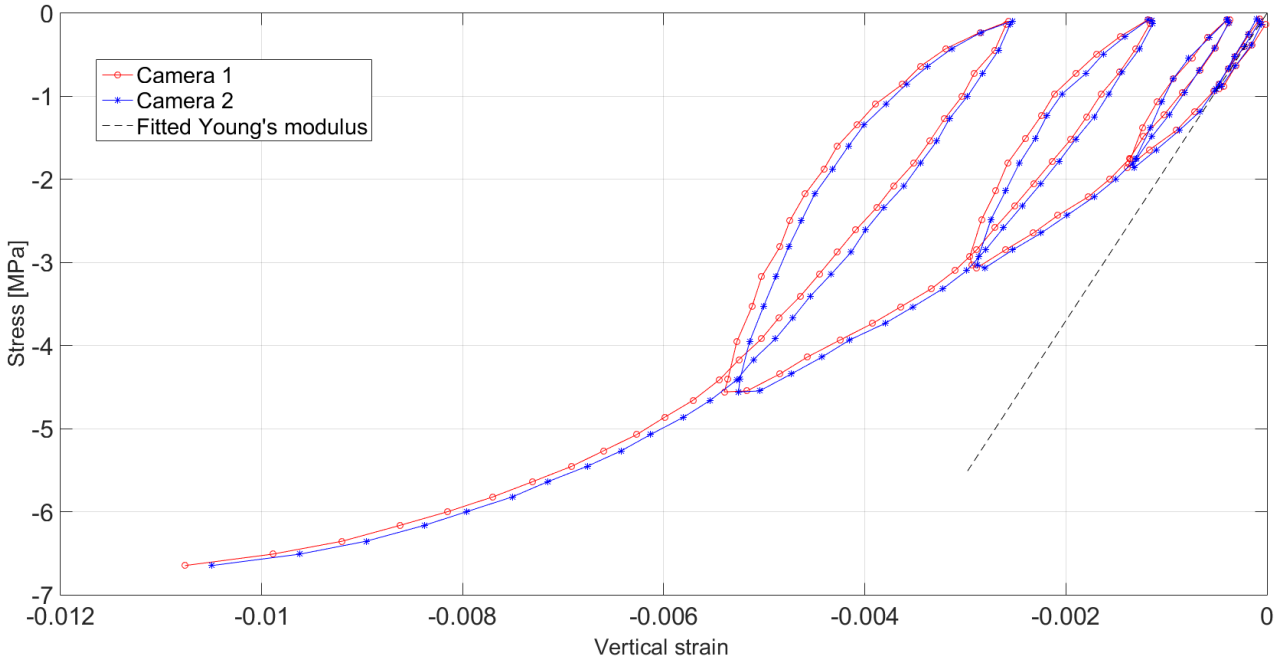

Figure 9 – Graph of the deviatoric strain by volumetric strain for uniaxial specimen U3. Arrows were added to highlight the beginning of the test and the dilatancy and fracture regions.

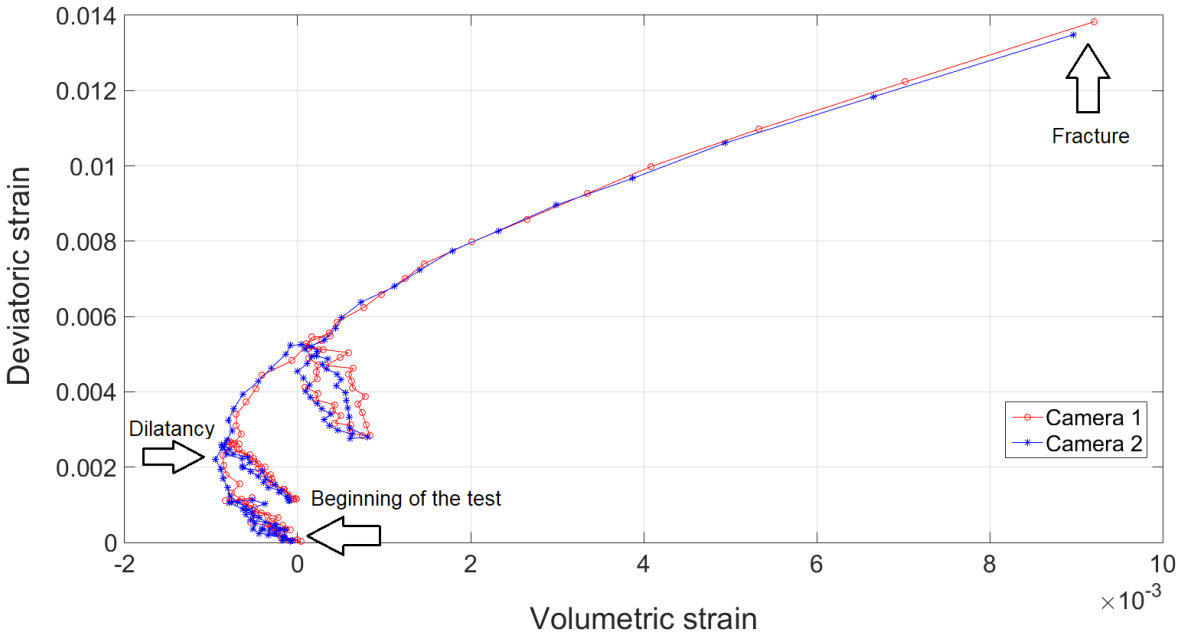

Figure 10 – Cycled diametral compression test of specimen D3 — average from cameras 1 and 2.

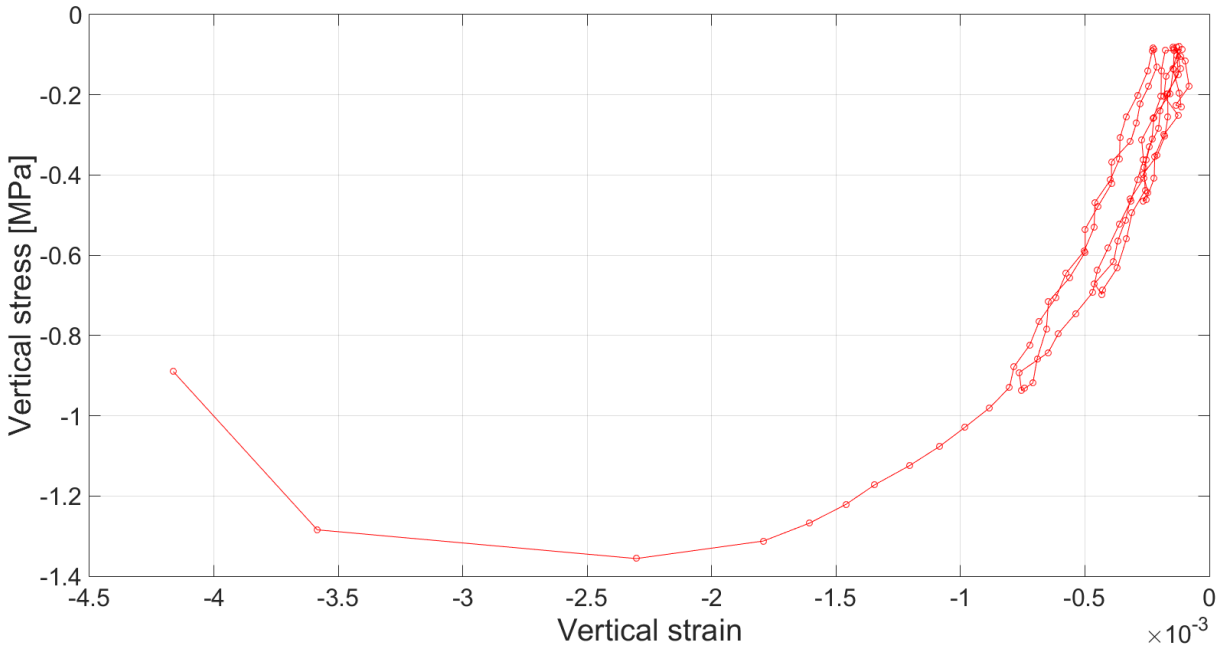

Figure 11 – Graph of the deviatoric strain by volumetric strain for diametral specimen D3 Average result from cameras 1 and 2. Arrows were added to highlight the dilatancy and fracture regions.

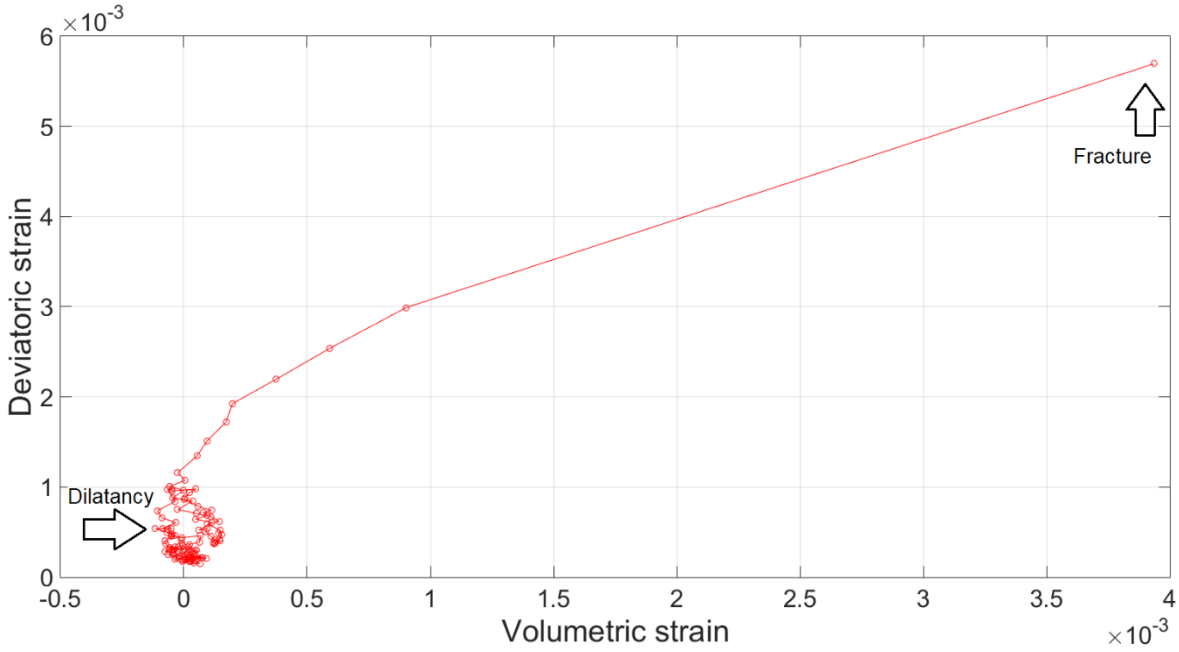

Figure 12 – Drucker-Prager failure surface adjusted to the uniaxial and diametral compression tests results, considering the dilatancy stress (blue) and fracture stress (red).

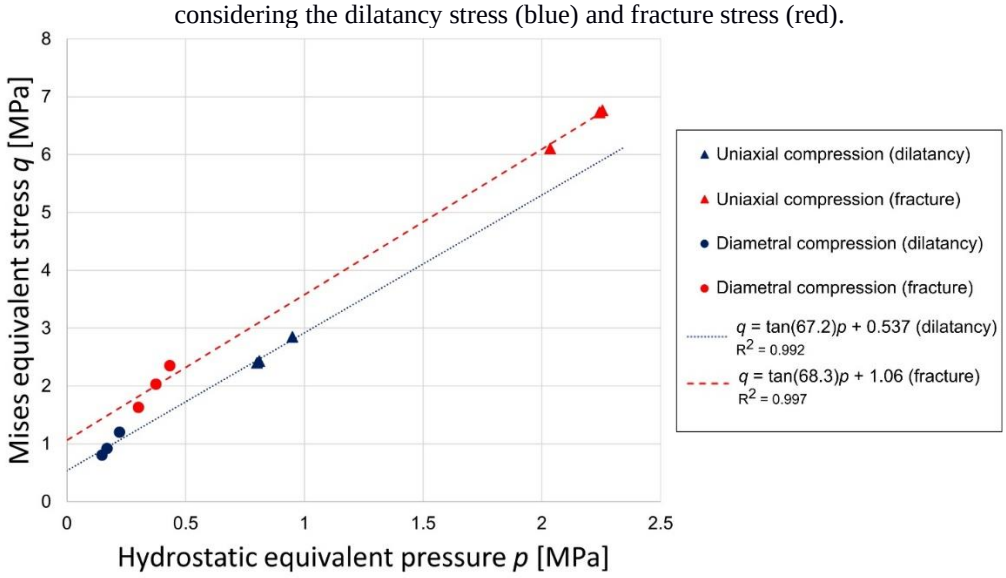

Figure 13 – Cap hardening fit.

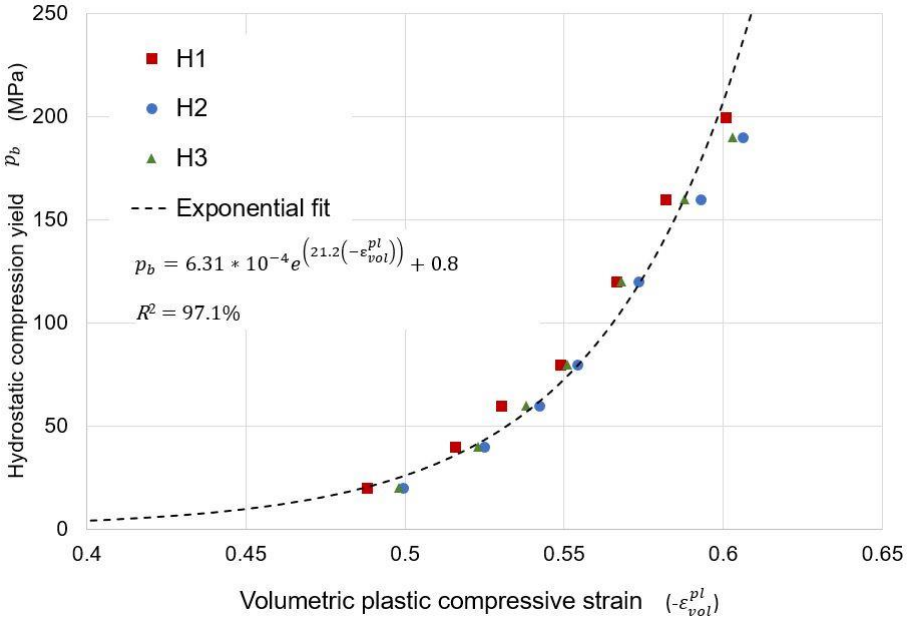

Figure 14 – Two compacted PZT hemispheres evidencing external and internal surfaces.

Figure 15 – On the left – density field resultant of the FE simulation with hardening and dilatancy. On the right – comparison between the measured profile and the simulations with and without hardening.

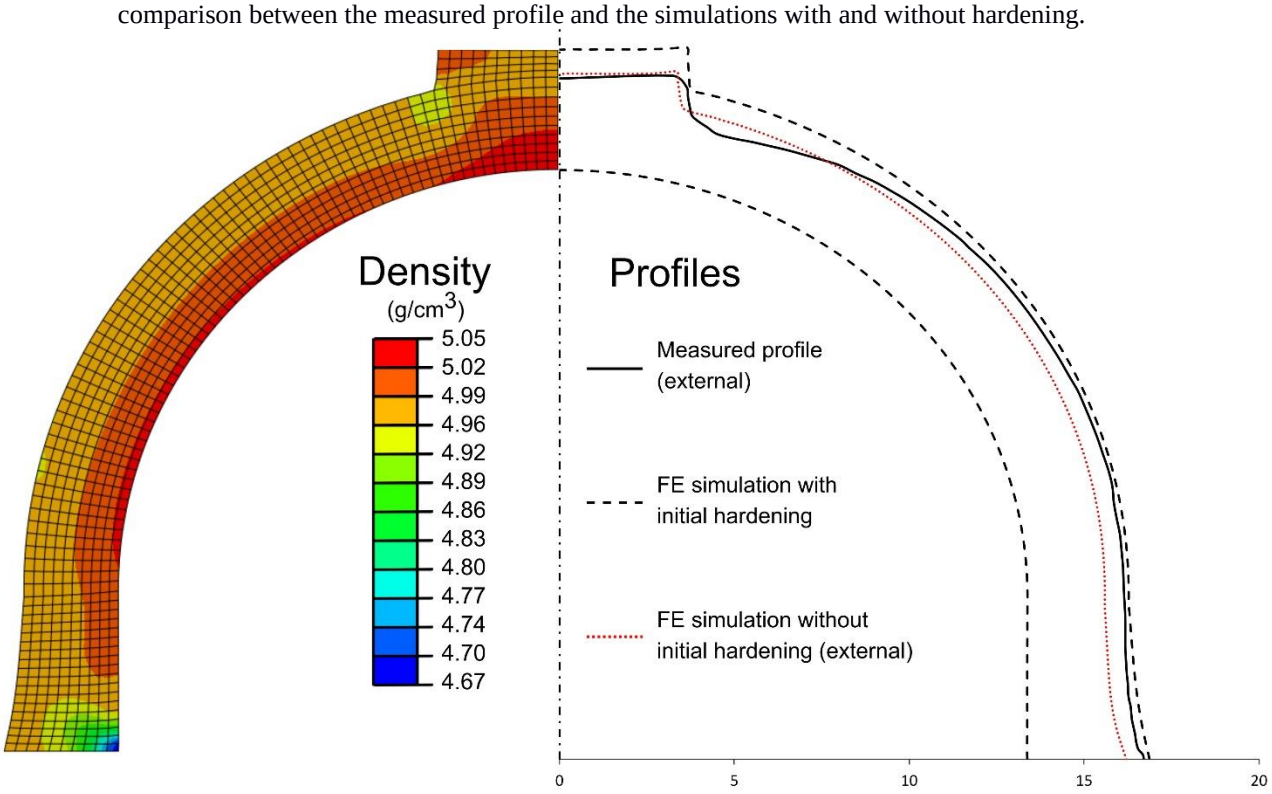

Figure 16 – Detail of the bottom of the part shaped as "elephant foot." A – simulated density field. B – projected profiled of the part (white dashed line added to highlight profile).

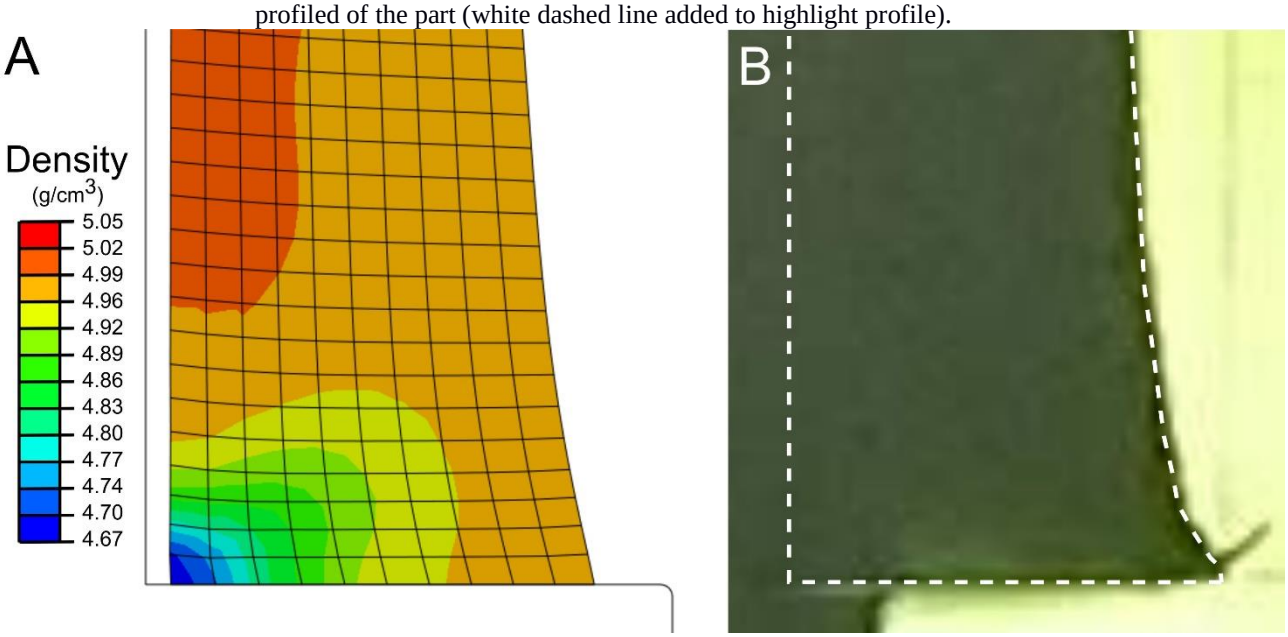

Figure 17 – Plastic strain caused by shear failure. On the left – simulation with parameters calibrated using fracture data. On the right – simulation with dilatancy data. The bottom region was magnified for improved comparison.

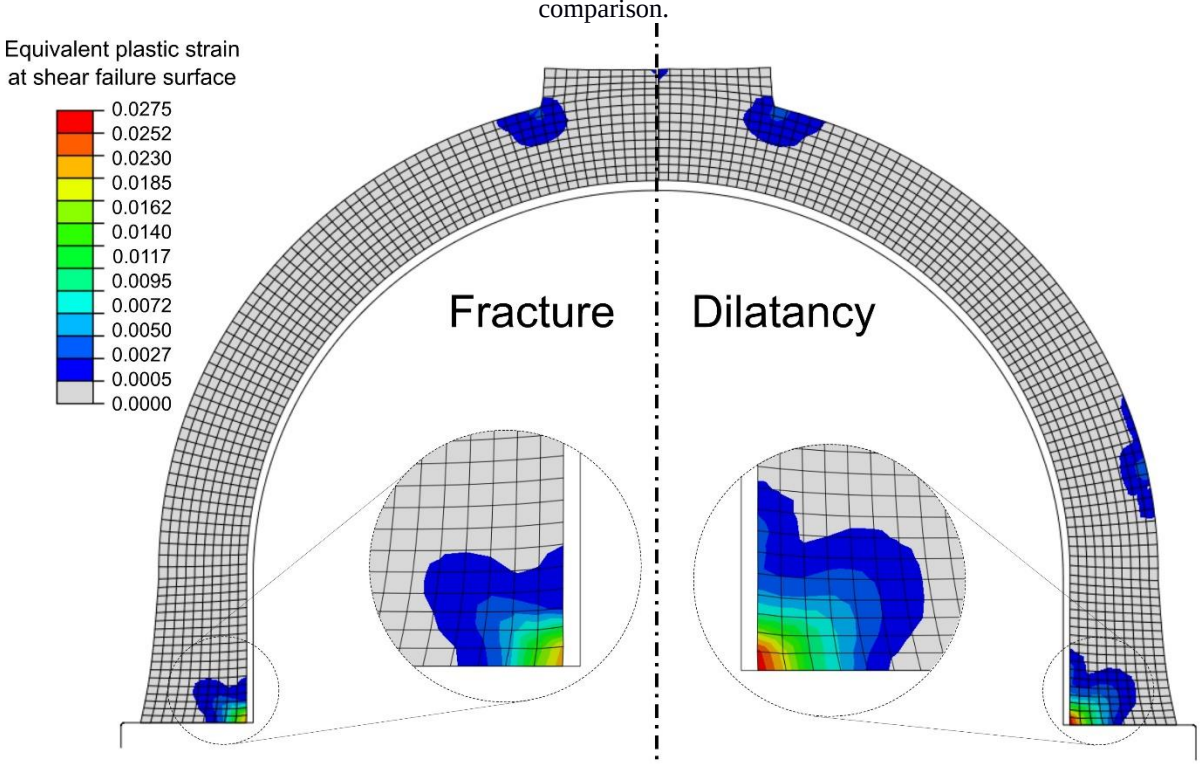

SUPPLEMENTARY MATERIAL S1-PZT-DilatancyHardening-Ext

```
*Heading
** Job name: PZT-S1-DilatancyHardening-Ext Model name: PZT_Hemisphere-NewHardening
** Generated by: Abaqus/CAE Student Edition 2019
*Preprint, echo=NO, model=NO, history=NO, contact=NO
**
** PARTS
**
*Part, name=Hemisphere
*Node
      1, 0.00400000019, 0.0165227111
      2, 0.00310117658, 0.0128099611
      3, 0.0131799998,          0.
      4, 0.0170000009,          0.
      5,          0., 0.0170000009
      6, 0.00400000019, 0.0179999992
      7,          0., 0.0179999992
      8, 0.0174000002, -0.00400000019
      9, 0.0131799998, -0.00400000019
     10, 0.0131799998, -0.00499999989
     11, 0.0175000001, -0.00499999989
     12,          0., 0.0131799998
     13, 0.00391011778, 0.0161514357
     14, 0.00382023538, 0.0157801621
     15, 0.00373035297, 0.0154088866
     16, 0.00364047056, 0.0150376111
     17, 0.00355058815, 0.0146663366
     18, 0.00346070598, 0.0142950611
     19, 0.00337082357, 0.0139237866
     20, 0.00328094116, 0.0135525111
     21, 0.00319105876, 0.0131812366
     22, 0.0034107659, 0.0127310278
     23, 0.00371835101, 0.0126446141
     24, 0.00402375124, 0.0125507703
     25, 0.00432678731, 0.0124495504
     26, 0.0046272804,  0.012341016
     27, 0.0049250545, 0.0122252293
     28, 0.00521993497, 0.0121022593
     29, 0.00551174767, 0.0119721778
     30, 0.00580032216,  0.011835061
     31, 0.00608548755, 0.0116909901
     32, 0.00636707759, 0.0115400488
     33, 0.00664492603, 0.0113823265
     34, 0.00691886991, 0.0112179164
     35, 0.0071887481, 0.0110469135
     36, 0.00745440181, 0.0108694201
     37, 0.00771567551, 0.0106855389
     38, 0.00797241554, 0.0104953796
     39, 0.00822447054,  0.010299053
     40, 0.00847169291, 0.0100966739
```

41, 0.00871393643, 0.00988836214
42, 0.00895106047, 0.0096742399
43, 0.0091829244, 0.00945443287
44, 0.00940939225, 0.00922907051
45, 0.00963033084, 0.00899828412
46, 0.00984561071, 0.00876221154
47, 0.0100551052, 0.00852098875
48, 0.0102586914, 0.0082747601
49, 0.0104562491, 0.00802366808
50, 0.0106476629, 0.00776786171
51, 0.0108328192, 0.00750749093
52, 0.0110116107, 0.00724270847
53, 0.0111839315, 0.00697367033
54, 0.0113496799, 0.00670053437
55, 0.01150876, 0.00642346079
56, 0.0116610769, 0.00614261255
57, 0.0118065411, 0.00585815543
58, 0.0119450679, 0.00557025522
59, 0.0120765762, 0.00527908234
60, 0.0122009879, 0.00498480722
61, 0.0123182293, 0.0046876031
62, 0.0124282334, 0.00438764459
63, 0.0125309341, 0.00408510724
64, 0.0126262708, 0.00378017011
65, 0.0127141885, 0.00347301131
66, 0.0127946353, 0.00316381175
67, 0.0128675634, 0.00285275304
68, 0.0129329311, 0.00254001818
69, 0.0129906991, 0.00222579064
70, 0.0130408332, 0.00191025529
71, 0.0130833043, 0.00159359735
72, 0.0131180873, 0.00127600308
73, 0.0131451618, 0.00095765898
74, 0.0131645128, 0.000638752128
75, 0.0131761273, 0.000319469924
76, 0.0135620004, 0.
77, 0.013944, 0.
78, 0.0143259997, 0.
79, 0.0147080002, 0.
80, 0.0150899999, 0.
81, 0.0154720005, 0.
82, 0.0158539992, 0.
83, 0.0162359998, 0.
84, 0.0166180003, 0.
85, 0.0169950053, 0.000412062858
86, 0.0169800241, 0.000823883631
87, 0.0169550646, 0.00123522023
88, 0.0169201437, 0.00164583104
89, 0.0168752782, 0.00205547456
90, 0.0168204978, 0.0024639105
91, 0.0167558324, 0.00287089846
92, 0.0166813228, 0.00327619957

93, 0.0165970102, 0.0036795754
94, 0.0165029448, 0.00408078916
95, 0.0163991805, 0.00447960477
96, 0.0162857827, 0.00487578847
97, 0.0161628127, 0.00526910694
98, 0.016030347, 0.00565932877
99, 0.01588846, 0.00604622578
100, 0.0157372374, 0.00642956933
101, 0.0155767677, 0.00680913497
102, 0.0154071441, 0.00718469964
103, 0.0152284671, 0.00755604263
104, 0.0150408428, 0.00792294554
105, 0.0148443794, 0.00828519184
106, 0.0146391932, 0.00864257105
107, 0.0144254044, 0.00899487082
108, 0.0142031396, 0.00934188534
109, 0.0139725292, 0.00968341064
110, 0.0137337074, 0.0100192456
111, 0.0134868165, 0.0103491927
112, 0.0132319992, 0.0106730592
113, 0.0129694073, 0.0109906532
114, 0.0126991952, 0.0113017894
115, 0.0124215195, 0.0116062844
116, 0.012136546, 0.0119039603
117, 0.0118444394, 0.01219464
118, 0.0115453741, 0.0124781542
119, 0.011239524, 0.0127543369
120, 0.010927069, 0.0130230244
121, 0.0106081944, 0.0132840592
122, 0.0102830846, 0.0135372877
123, 0.00995193329, 0.0137825618
124, 0.00961493421, 0.014019738
125, 0.00927228481, 0.0142486747
126, 0.00892418716, 0.0144692389
127, 0.00857084524, 0.0146813011
128, 0.00821246766, 0.0148847364
129, 0.00784926303, 0.0150794256
130, 0.00748144696, 0.0152652534
131, 0.00710923458, 0.0154421106
132, 0.00673284475, 0.0156098939
133, 0.00635249866, 0.0157685056
134, 0.00596841937, 0.0159178507
135, 0.00558083318, 0.0160578415
136, 0.00518996734, 0.016188398
137, 0.00479605235, 0.016309442
138, 0.00439931871, 0.0164209008
139, 0.00040374801, 0.0169952046
140, 0.000807268254, 0.0169808213
141, 0.00121033308, 0.0169568602
142, 0.00161271519, 0.0169233307
143, 0.0020141874, 0.0168802571
144, 0.00241452339, 0.0168276578

145, 0.00281349733, 0.0167655665
146, 0.00321088405, 0.0166940168
147, 0.00360645936, 0.0166130513
148, 0.00400000019, 0.0168920346
149, 0.00400000019, 0.0172613561
150, 0.00400000019, 0.0176306777
151, 0.00359999994, 0.0179999992
152, 0.00319999992, 0.0179999992
153, 0.0027999999, 0.0179999992
154, 0.00240000011, 0.0179999992
155, 0.00200000009, 0.0179999992
156, 0.00159999996, 0.0179999992
157, 0.00120000006, 0.0179999992
158, 0.00079999998, 0.0179999992
159, 0.00039999999, 0.0179999992
160, 0., 0.0177500006
161, 0., 0.0175000001
162, 0., 0.0172499996
163, 0.0169779994, -0.00400000019
164, 0.0165560003, -0.00400000019
165, 0.0161339995, -0.00400000019
166, 0.0157120004, -0.00400000019
167, 0.0152899995, -0.00400000019
168, 0.0148679996, -0.00400000019
169, 0.0144459996, -0.00400000019
170, 0.0140239997, -0.00400000019
171, 0.0136019997, -0.00400000019
172, 0.0131799998, -0.00425000023
173, 0.0131799998, -0.00449999981
174, 0.0131799998, -0.00474999985
175, 0.0136120003, -0.00499999989
176, 0.0140439998, -0.00499999989
177, 0.0144760003, -0.00499999989
178, 0.0149079999, -0.00499999989
179, 0.0153400004, -0.00499999989
180, 0.015772, -0.00499999989
181, 0.0162039995, -0.00499999989
182, 0.0166359991, -0.00499999989
183, 0.0170680005, -0.00499999989
184, 0.0174749997, -0.00474999985
185, 0.0174499992, -0.00449999981
186, 0.0174250007, -0.00425000023
187, 0.0173714291, -0.00371428579
188, 0.017342858, -0.00342857139
189, 0.017314285, -0.00314285723
190, 0.0172857139, -0.00285714283
191, 0.0172571428, -0.00257142866
192, 0.0172285717, -0.00228571426
193, 0.0172000006, -0.00200000009
194, 0.0171714295, -0.0017142857
195, 0.0171428565, -0.00142857141
196, 0.0171142854, -0.00114285713

197, 0.0170857143, -0.000857142848
198, 0.0170571432, -0.000571428565
199, 0.017028572, -0.000285714283
200, 0.0131799998, -0.000285714283
201, 0.0131799998, -0.000571428565
202, 0.0131799998, -0.000857142848
203, 0.0131799998, -0.00114285713
204, 0.0131799998, -0.00142857141
205, 0.0131799998, -0.0017142857
206, 0.0131799998, -0.00200000009
207, 0.0131799998, -0.00228571426
208, 0.0131799998, -0.00257142866
209, 0.0131799998, -0.00285714283
210, 0.0131799998, -0.00314285723
211, 0.0131799998, -0.00342857139
212, 0.0131799998, -0.00371428579
213,   0., 0.0166180003
214,   0., 0.0162359998
215,   0., 0.0158539992
216,   0., 0.0154720005
217,   0., 0.0150899999
218,   0., 0.0147080002
219,   0., 0.0143259997
220,   0.,   0.013944
221,   0., 0.0135620004
222, 0.000313023455, 0.0131762819
223, 0.000625870365, 0.0131651312
224, 0.00093836413, 0.0131465532
225, 0.00125032861, 0.013120559
226, 0.00156158768, 0.0130871637
227, 0.00187196583, 0.0130463848
228, 0.00218128785, 0.0129982457
229, 0.00248937937, 0.0129427733
230, 0.00279606669, 0.0128800003
231, 0.00430046348, 0.0160519145
232, 0.00420160824, 0.0156829264
233, 0.00410275301, 0.0153139392
234, 0.00400389731, 0.014944952
235, 0.00390504231, 0.0145759648
236, 0.00380618707, 0.0142069776
237, 0.00370733161, 0.0138379904
238, 0.00360847637, 0.0134690031
239, 0.00350962114, 0.013100015
240, 0.00468828203, 0.0159429591
241, 0.00458051218, 0.0155764762
242, 0.00447274186, 0.0152099933
243, 0.00436497154, 0.0148435105
244, 0.00425720168, 0.0144770276
245, 0.00414943136, 0.0141105447
246, 0.00404166151, 0.0137440627
247, 0.00393389119, 0.0133775799
248, 0.0038261211, 0.013011097

249, 0.00507334573, 0.0158246346
250, 0.00495672412, 0.015460873
251, 0.00484010251, 0.0150971096
252, 0.0047234809, 0.0147333471
253, 0.00460685929, 0.0143695837
254, 0.00449023768, 0.0140058212
255, 0.00437361607, 0.0136420587
256, 0.00425699446, 0.0132782953
257, 0.00414037285, 0.0129145328
258, 0.00545542873, 0.0156970136
259, 0.00533002382, 0.0153361838
260, 0.00520461937, 0.014975355
261, 0.00507921493, 0.0146145262
262, 0.00495381001, 0.0142536964
263, 0.00482840557, 0.0138928676
264, 0.00470300112, 0.0135320378
265, 0.00457759621, 0.013171209
266, 0.00445219176, 0.0128103802
267, 0.00583430566, 0.0155601669
268, 0.00570019148, 0.0152024841
269, 0.00556607777, 0.0148448003
270, 0.0054319636, 0.0144871166
271, 0.00529784989, 0.0141294338
272, 0.00516373618, 0.01377175
273, 0.005029622, 0.0134140663
274, 0.00489550829, 0.0130563825
275, 0.00476139411, 0.0126986997
276, 0.00620975392, 0.0154141774
277, 0.00606700964, 0.0150598502
278, 0.00592426537, 0.0147055229
279, 0.00578152109, 0.0143511947
280, 0.00563877635, 0.0139968675
281, 0.00549603207, 0.0136425402
282, 0.00535328779, 0.013288212
283, 0.00521054352, 0.0129338847
284, 0.00506779924, 0.0125795575
285, 0.00658155372, 0.0152591309
286, 0.0064302627, 0.0149083678
287, 0.00627897168, 0.0145576037
288, 0.00612768065, 0.0142068407
289, 0.00597638963, 0.0138560766
290, 0.0058250986, 0.0135053135
291, 0.00567380805, 0.0131545495
292, 0.00552251702, 0.0128037864
293, 0.005371226, 0.0124530224
294, 0.00694948575, 0.0150951175
295, 0.00678973738, 0.0147481244
296, 0.00662998855, 0.0144011304
297, 0.00647023972, 0.0140541373
298, 0.00631049136, 0.0137071442
299, 0.00615074253, 0.0133601511
300, 0.0059909937, 0.0130131571

301, 0.00583124533, 0.012666164
302, 0.0056714965, 0.0123191709
303, 0.00731333438, 0.0149222342
304, 0.00714522228, 0.0145792142
305, 0.0069771097, 0.014236195
306, 0.00680899713, 0.0138931759
307, 0.00664088456, 0.0135501567
308, 0.00647277199, 0.0132071376
309, 0.00630465942, 0.0128641184
310, 0.00613654684, 0.0125210993
311, 0.00596843427, 0.0121780802
312, 0.0076728859, 0.0147405816
313, 0.0074965083, 0.0144017385
314, 0.00732013071, 0.0140628945
315, 0.00714375312, 0.0137240514
316, 0.00696737552, 0.0133852074
317, 0.00679099793, 0.0130463643
318, 0.00661462033, 0.0127075203
319, 0.00643824274, 0.0123686772
320, 0.00626186514, 0.0120298332
321, 0.00802792795, 0.0145502677
322, 0.00784338918, 0.014215799
323, 0.0076588504, 0.0138813304
324, 0.00747431116, 0.0135468617
325, 0.00728977239, 0.013212393
326, 0.00710523361, 0.0128779234
327, 0.00692069437, 0.0125434548
328, 0.0067361556, 0.0122089861
329, 0.00655161636, 0.0118745174
330, 0.00837825332, 0.0143514043
331, 0.0081856614, 0.0140215065
332, 0.00799306948, 0.0136916088
333, 0.00780047756, 0.0133617111
334, 0.00760788564, 0.0130318142
335, 0.00741529372, 0.0127019165
336, 0.0072227018, 0.0123720188
337, 0.00703010987, 0.012042122
338, 0.00683751795, 0.0117122242
339, 0.00872365572, 0.0141441068
340, 0.00852312334, 0.0138189746
341, 0.00832259189, 0.0134938424
342, 0.00812206045, 0.0131687103
343, 0.00792152807, 0.0128435772
344, 0.00772099663, 0.012518445
345, 0.00752046518, 0.0121933129
346, 0.00731993327, 0.0118681807
347, 0.00711940136, 0.0115430485
348, 0.00906393118, 0.0139284991
349, 0.00885557756, 0.0136083225
350, 0.00864722393, 0.0132881468
351, 0.00843887031, 0.0129679702
352, 0.00823051669, 0.0126477946

353, 0.00802216306, 0.012327618
354, 0.00781380944, 0.0120074423
355, 0.00760545535, 0.0116872657
356, 0.00739710173, 0.01136709
357, 0.00939888135, 0.013704706
358, 0.00918282755, 0.013389674
359, 0.00896677468, 0.013074642
360, 0.00875072088, 0.0127596101
361, 0.00853466801, 0.012444579
362, 0.00831861515, 0.0121295471
363, 0.00810256135, 0.0118145151
364, 0.00788650848, 0.0114994831
365, 0.00767045515, 0.0111844521
366, 0.00972830784, 0.0134728597
367, 0.00950468238, 0.0131631577
368, 0.009281056, 0.0128534557
369, 0.00905743055, 0.0125437528
370, 0.00883380417, 0.0122340508
371, 0.00861017872, 0.0119243488
372, 0.00838655327, 0.0116146458
373, 0.00816292688, 0.0113049438
374, 0.00793930143, 0.0109952418
375, 0.0100520179, 0.0132330973
376, 0.00982095115, 0.0129289059
377, 0.00958988443, 0.0126247155
378, 0.00935881678, 0.012320525
379, 0.00912775006, 0.0120163336
380, 0.00889668334, 0.0117121432
381, 0.00866561662, 0.0114079518
382, 0.00843454897, 0.0111037614
383, 0.00820348226, 0.01079957
384, 0.0103698215, 0.0129855582
385, 0.0101314494, 0.0126870573
386, 0.00989307649, 0.0123885572
387, 0.00965470448, 0.0120900562
388, 0.00941633247, 0.0117915561
389, 0.00917795952, 0.0114930551
390, 0.00893958751, 0.0111945542
391, 0.0087012155, 0.0108960541
392, 0.00846284255, 0.0105975531
393, 0.0106815314, 0.0127303889
394, 0.0104359938, 0.0124377543
395, 0.0101904562, 0.0121451188
396, 0.00994491857, 0.0118524842
397, 0.00969938096, 0.0115598487
398, 0.00945384335, 0.0112672141
399, 0.00920830574, 0.0109745786
400, 0.00896276813, 0.010681944
401, 0.00871723052, 0.0103893084
402, 0.0109869651, 0.0124677392
403, 0.0107344063, 0.0121811414
404, 0.0104818475, 0.0118945446

405, 0.0102292895, 0.0116079468
406, 0.00997673068, 0.0113213491
407, 0.00972417183, 0.0110347522
408, 0.00947161298, 0.0107481545
409, 0.00921905413, 0.0104615567
410, 0.00896649528, 0.0101749599
411, 0.011285943, 0.0121977627
412, 0.011026511, 0.0119173713
413, 0.0107670799, 0.0116369799
414, 0.0105076488, 0.0113565885
415, 0.0102482168, 0.011076197
416, 0.00998878572, 0.0107958056
417, 0.00972935464, 0.0105154142
418, 0.00946992356, 0.0102350228
419, 0.00921049155, 0.00995463133
420, 0.0115782879, 0.0119206198
421, 0.0113121364, 0.0116465986
422, 0.0110459849, 0.0113725783
423, 0.0107798334, 0.0110985572
424, 0.0105136819, 0.010824536
425, 0.0102475304, 0.0105505157
426, 0.00998137891, 0.0102764945
427, 0.00971522741, 0.0100024743
428, 0.00944907591, 0.00972845312
429, 0.0118638305, 0.0116364714
430, 0.011591115, 0.0113689816
431, 0.0113183996, 0.0111014927
432, 0.0110456841, 0.0108340038
433, 0.0107729686, 0.0105665149
434, 0.0105002532, 0.010299026
435, 0.0102275386, 0.0100315372
436, 0.00995482318, 0.00976404827
437, 0.00968210772, 0.00949655939
438, 0.0121424012, 0.0113454852
439, 0.011863282, 0.0110846851
440, 0.0115841627, 0.010823885
441, 0.0113050444, 0.0105630849
442, 0.0110259252, 0.0103022847
443, 0.0107468069, 0.0100414846
444, 0.0104676876, 0.00978068449
445, 0.0101885693, 0.00951988436
446, 0.00990945008, 0.00925908424
447, 0.0124138361, 0.0110478317
448, 0.0121284779, 0.010793874
449, 0.0118431197, 0.0105399163
450, 0.0115577616, 0.0102859586
451, 0.0112724034, 0.010032
452, 0.0109870443, 0.00977804232
453, 0.0107016861, 0.00952408463
454, 0.010416328, 0.00927012693
455, 0.0101309698, 0.00901616924
456, 0.0126779778, 0.0107436869

457, 0.0123865474, 0.0104967207
458, 0.012095117, 0.0102497544
459, 0.0118036866, 0.0100027872
460, 0.0115122562, 0.00975582097
461, 0.0112208268, 0.00950885471
462, 0.0109293964, 0.00926188845
463, 0.010637966, 0.00901492219
464, 0.0103465356, 0.00876795501
465, 0.0129346689, 0.0104332287
466, 0.0126373377, 0.0101933992
467, 0.0123400073, 0.00995356962
468, 0.0120426761, 0.00971373916
469, 0.0117453458, 0.00947390962
470, 0.0114480145, 0.00923407916
471, 0.0111506842, 0.00899424963
472, 0.010853353, 0.00875442009
473, 0.0105560226, 0.00851458963
474, 0.0131837595, 0.0101166405
475, 0.0128807025, 0.0098840883
476, 0.0125776464, 0.00965153519
477, 0.0122745894, 0.00941898301
478, 0.0119715324, 0.00918643083
479, 0.0116684763, 0.00895387772
480, 0.0113654193, 0.00872132555
481, 0.0110623622, 0.00848877337
482, 0.0107593061, 0.00825622119
483, 0.0134251034, 0.00979410671
484, 0.0131164985, 0.00956896879
485, 0.0128078945, 0.00934382994
486, 0.0124992896, 0.00911869202
487, 0.0121906847, 0.00889355317
488, 0.0118820807, 0.00866841525
489, 0.0115734758, 0.00844327733
490, 0.0112648718, 0.00821813848
491, 0.0109562669, 0.00799300056
492, 0.013658558, 0.00946581829
493, 0.0133445868, 0.00924822688
494, 0.0130306156, 0.00903063454
495, 0.0127166454, 0.00881304219
496, 0.0124026742, 0.00859545078
497, 0.012088703, 0.00837785844
498, 0.0117747327, 0.00816026703
499, 0.0114607615, 0.00794267468
500, 0.0111467903, 0.0077250828
501, 0.0138839865, 0.00913196802
502, 0.0135648344, 0.00892204978
503, 0.0132456813, 0.00871213246
504, 0.0129265282, 0.00850221422
505, 0.0126073752, 0.0082922969
506, 0.0122882221, 0.00808237959
507, 0.011969069, 0.00787246134
508, 0.0116499169, 0.00766254403

509, 0.0113307638, 0.00745262625
510, 0.0141012575, 0.00879275054
511, 0.0137771098, 0.00859063026
512, 0.013452963, 0.00838851091
513, 0.0131288152, 0.00818639062
514, 0.0128046684, 0.00798427034
515, 0.0124805206, 0.00778215053
516, 0.0121563738, 0.00758003071
517, 0.0118322261, 0.00737791043
518, 0.0115080783, 0.00717579061
519, 0.0143102417, 0.00844836701
520, 0.0139812902, 0.00825416297
521, 0.0136523396, 0.00805995986
522, 0.0133233881, 0.00786575582
523, 0.0129944365, 0.00767155224
524, 0.012665485, 0.00747734867
525, 0.0123365344, 0.0072831451
526, 0.0120075829, 0.00708894152
527, 0.0116786314, 0.00689473795
528, 0.0145108169, 0.0080990186
529, 0.0141772553, 0.00791284628
530, 0.0138436938, 0.00772667257
531, 0.0135101313, 0.00754049979
532, 0.0131765697, 0.00735432655
533, 0.0128430072, 0.0071681533
534, 0.0125094457, 0.00698198006
535, 0.0121758841, 0.00679580681
536, 0.0118423216, 0.00660963403
537, 0.0147028659, 0.00774491206
538, 0.0143648889, 0.00756687857
539, 0.0140269129, 0.00738884555
540, 0.0136889359, 0.00721081207
541, 0.0133509599, 0.00703277905
542, 0.0130129829, 0.00685474556
543, 0.0126750059, 0.00667671254
544, 0.0123370299, 0.00649867905
545, 0.0119990529, 0.00632064603
546, 0.0148862749, 0.00738625368
547, 0.0145440819, 0.00721646519
548, 0.0142018897, 0.00704667624
549, 0.0138596967, 0.00687688775
550, 0.0135175046, 0.0067070988
551, 0.0131753115, 0.00653731031
552, 0.0128331194, 0.00636752136
553, 0.0124909263, 0.00619773287
554, 0.0121487342, 0.00602794392
555, 0.0150609361, 0.00702325534
556, 0.014714729, 0.00686181104
557, 0.014368521, 0.00670036627
558, 0.014022314, 0.00653892197
559, 0.013676106, 0.00637747766
560, 0.0133298989, 0.00621603336

561, 0.0129836909, 0.00605458859
562, 0.012637483, 0.00589314429
563, 0.0122912759, 0.00573169999
564, 0.0152267478, 0.00665612984
565, 0.0148767289, 0.00650312472
566, 0.0145267099, 0.00635011913
567, 0.014176691, 0.00619711401
568, 0.013826672, 0.00604410889
569, 0.0134766521, 0.0058911033
570, 0.0131266331, 0.00573809817
571, 0.0127766142, 0.00558509305
572, 0.0124265952, 0.00543208746
573, 0.0153836124, 0.00628509326
574, 0.0150299873, 0.00614061719
575, 0.0146763623, 0.00599614065
576, 0.0143227372, 0.00585166458
577, 0.0139691122, 0.00570718851
578, 0.0136154871, 0.00556271197
579, 0.0132618621, 0.0054182359
580, 0.0129082371, 0.00527375983
581, 0.012554612, 0.00512928376
582, 0.0155314365, 0.00591036351
583, 0.015174414, 0.00577450125
584, 0.0148173906, 0.00563863898
585, 0.0144603681, 0.00550277671
586, 0.0141033446, 0.00536691444
587, 0.0137463212, 0.00523105217
588, 0.0133892987, 0.0050951899
589, 0.0130322753, 0.00495932763
590, 0.0126752527, 0.00482346537
591, 0.0156701356, 0.0055321604
592, 0.0153099233, 0.00540499203
593, 0.014949712, 0.00527782366
594, 0.0145895006, 0.00515065528
595, 0.0142292893, 0.00502348645
596, 0.0138690779, 0.00489631807
597, 0.0135088665, 0.0047691497
598, 0.0131486561, 0.00464198133
599, 0.0127884448, 0.00451481296
600, 0.0157996248, 0.00515070697
601, 0.015436437, 0.005032307
602, 0.0150732491, 0.00491390703
603, 0.0147100613, 0.00479550706
604, 0.0143468734, 0.00467710709
605, 0.0139836855, 0.00455870712
606, 0.0136204977, 0.00444030715
607, 0.0132573098, 0.00432190718
608, 0.0128941219, 0.00420350721
609, 0.0159198307, 0.00476622628
610, 0.0155538796, 0.00465666456
611, 0.0151879285, 0.00454710284
612, 0.0148219774, 0.00443754112

613, 0.0144560263, 0.00432797894
614, 0.0140900752, 0.00421841722
615, 0.0137241241, 0.0041088555
616, 0.013358173, 0.00399929378
617, 0.0129922219, 0.00388973183
618, 0.0160306823, 0.00437894557
619, 0.0156621821, 0.00427828589
620, 0.0152936829, 0.00417762669
621, 0.0149251837, 0.00407696748
622, 0.0145566845, 0.00397630828
623, 0.0141881853, 0.0038756486
624, 0.0138196861, 0.0037749894
625, 0.0134511869, 0.00367432996
626, 0.0130826877, 0.00357367075
627, 0.0161321126, 0.00398909114
628, 0.0157612823, 0.00389739359
629, 0.0153904511, 0.0038056958
630, 0.0150196208, 0.00371399825
631, 0.0146487895, 0.00362230046
632, 0.0142779592, 0.00353060267
633, 0.013907128, 0.00343890488
634, 0.0135362968, 0.00334720733
635, 0.0131654665, 0.00325550954
636, 0.0162240658, 0.00359689305
637, 0.0158511195, 0.00351421093
638, 0.0154781761, 0.00343152881
639, 0.0151052317, 0.00334884645
640, 0.0147322863, 0.00326616433
641, 0.0143593419, 0.00318348198
642, 0.0139863975, 0.00310079986
643, 0.0136134531, 0.00301811751
644, 0.0132405087, 0.00293543539
645, 0.0163064841, 0.00320258131
646, 0.0159316435, 0.00312896329
647, 0.0155568048, 0.00305534503
648, 0.0151819661, 0.00298172701
649, 0.0148071265, 0.00290810876
650, 0.0144322878, 0.00283449073
651, 0.0140574481, 0.00276087248
652, 0.0136826094, 0.00268725445
653, 0.0133077707, 0.00261363643
654, 0.0163793191, 0.00280638761
655, 0.0160028059, 0.00274187699
656, 0.0156262927, 0.00267736614
657, 0.0152497794, 0.00261285529
658, 0.0148732662, 0.00254834467
659, 0.0144967521, 0.00248383381
660, 0.0141202388, 0.00241932296
661, 0.0137437256, 0.00235481234
662, 0.0133672124, 0.00229030149
663, 0.0164425317, 0.002408545
664, 0.0160645656, 0.0023531795

665, 0.0156865977, 0.002297814
666, 0.0153086316, 0.00224244851
667, 0.0149306655, 0.00218708278
668, 0.0145526985, 0.00213171728
669, 0.0141747324, 0.00207635178
670, 0.0137967663, 0.00202098629
671, 0.0134187993, 0.00196562079
672, 0.0164960809, 0.00200928701
673, 0.0161168836, 0.00196309923
674, 0.0157376863, 0.00191691145
675, 0.015358489, 0.00187072379
676, 0.0149792917, 0.00182453601
677, 0.0146000935, 0.00177834835
678, 0.0142208962, 0.00173216057
679, 0.0138416989, 0.00168597291
680, 0.0134625016, 0.00163978513
681, 0.0165399369, 0.00160884822
682, 0.0161597319, 0.0015718654
683, 0.0157795269, 0.00153488258
684, 0.015399321, 0.00149789988
685, 0.0150191151, 0.00146091706
686, 0.0146389101, 0.00142393424
687, 0.0142587041, 0.00138695142
688, 0.0138784982, 0.00134996872
689, 0.0134982932, 0.0013129859
690, 0.0165740754, 0.00120746414
691, 0.0161930844, 0.00117970794
692, 0.0158120934, 0.00115195184
693, 0.0154311042, 0.00112419575
694, 0.0150501132, 0.00109643955
695, 0.0146691231, 0.00106868346
696, 0.014288133, 0.00104092737
697, 0.0139071429, 0.00101317116
698, 0.0135261528, 0.00098541507
699, 0.0165984724, 0.000805370451
700, 0.0162169226, 0.00078685733
701, 0.0158353709, 0.000768344151
702, 0.0154538192, 0.00074983103
703, 0.0150722684, 0.00073131785
704, 0.0146907177, 0.000712804729
705, 0.014309166, 0.00069429155
706, 0.0139276152, 0.000675778429
707, 0.0135460636, 0.000657265249
708, 0.0166131184, 0.000402803562
709, 0.0162312295, 0.000393544266
710, 0.0158493426, 0.000384284998
711, 0.0154674537, 0.000375025702
712, 0.0150855668, 0.000365766406
713, 0.0147036789, 0.000356507109
714, 0.014321791, 0.000347247813
715, 0.0139399031, 0.000337988517
716, 0.0135580152, 0.00032872922

717, 0.000402811012, 0.0172464028
718, 0.000805451185, 0.0172356162
719, 0.00120774982, 0.0172176454
720, 0.00160953635, 0.0171924978
721, 0.00201064069, 0.0171601921
722, 0.00241089263, 0.0171207432
723, 0.00281012291, 0.0170741752
724, 0.00320816296, 0.0170205124
725, 0.00360484445, 0.0169597883
726, 0.000401874015, 0.0174976029
727, 0.000803634117, 0.0174904112
728, 0.00120516657, 0.0174784306
729, 0.00160635763, 0.017461665
730, 0.00200709375, 0.0174401272
731, 0.00240726164, 0.0174138285
732, 0.00280674873, 0.0173827838
733, 0.00320544187, 0.017347008
734, 0.00360322953, 0.0173065253
735, 0.000400937017, 0.017748801
736, 0.000801817048, 0.0177452061
737, 0.00120258331, 0.0177392159
738, 0.0016031788, 0.0177308321
739, 0.0020035468, 0.0177200641
740, 0.00240363088, 0.0177069139
741, 0.00280337431, 0.0176913925
742, 0.00320272101, 0.0176735036
743, 0.00360161485, 0.0176532622
744, 0.0170005001, -0.00425000023
745, 0.0165759996, -0.00425000023
746, 0.0161515009, -0.00425000023
747, 0.0157270003, -0.00425000023
748, 0.0153024998, -0.00425000023
749, 0.0148780001, -0.00425000023
750, 0.0144534996, -0.00425000023
751, 0.014029, -0.00425000023
752, 0.0136045003, -0.00425000023
753, 0.0170230009, -0.00449999981
754, 0.0165960006, -0.00449999981
755, 0.0161690004, -0.00449999981
756, 0.0157420002, -0.00449999981
757, 0.015315, -0.00449999981
758, 0.0148879997, -0.00449999981
759, 0.0144610004, -0.00449999981
760, 0.0140340002, -0.00449999981
761, 0.013607, -0.00449999981
762, 0.0170454998, -0.00474999985
763, 0.0166159999, -0.00474999985
764, 0.0161865, -0.00474999985
765, 0.0157570001, -0.00474999985
766, 0.0153275002, -0.00474999985
767, 0.0148980003, -0.00474999985
768, 0.0144685004, -0.00474999985

769, 0.0140389996, -0.00474999985
770, 0.0136094997, -0.00474999985
771, 0.0135991424, -0.00371428579
772, 0.014018286, -0.00371428579
773, 0.0144374287, -0.00371428579
774, 0.0148565713, -0.00371428579
775, 0.015275714, -0.00371428579
776, 0.0156948566, -0.00371428579
777, 0.0161140002, -0.00371428579
778, 0.016533142, -0.00371428579
779, 0.0169522855, -0.00371428579
780, 0.0135962861, -0.00342857139
781, 0.0140125714, -0.00342857139
782, 0.0144288568, -0.00342857139
783, 0.0148451431, -0.00342857139
784, 0.0152614284, -0.00342857139
785, 0.0156777147, -0.00342857139
786, 0.0160939991, -0.00342857139
787, 0.0165102854, -0.00342857139
788, 0.0169265717, -0.00342857139
789, 0.0135934288, -0.00314285723
790, 0.0140068568, -0.00314285723
791, 0.0144202858, -0.00314285723
792, 0.0148337139, -0.00314285723
793, 0.0152471429, -0.00314285723
794, 0.0156605709, -0.00314285723
795, 0.0160739999, -0.00314285723
796, 0.0164874289, -0.00314285723
797, 0.0169008579, -0.00314285723
798, 0.0135905715, -0.00285714283
799, 0.0140011432, -0.00285714283
800, 0.0144117139, -0.00285714283
801, 0.0148222856, -0.00285714283
802, 0.0152328573, -0.00285714283
803, 0.015643429, -0.00285714283
804, 0.0160540007, -0.00285714283
805, 0.0164645705, -0.00285714283
806, 0.0168751422, -0.00285714283
807, 0.0135877142, -0.00257142866
808, 0.0139954286, -0.00257142866
809, 0.014403143, -0.00257142866
810, 0.0148108574, -0.00257142866
811, 0.0152185718, -0.00257142866
812, 0.0156262852, -0.00257142866
813, 0.0160339996, -0.00257142866
814, 0.016441714, -0.00257142866
815, 0.0168494284, -0.00257142866
816, 0.0135848569, -0.00228571426
817, 0.013989714, -0.00228571426
818, 0.0143945711, -0.00228571426
819, 0.0147994282, -0.00228571426
820, 0.0152042853, -0.00228571426

821, 0.0156091433, -0.00228571426
822, 0.0160140004, -0.00228571426
823, 0.0164188575, -0.00228571426
824, 0.0168237146, -0.00228571426
825, 0.0135819996, -0.00200000009
826, 0.0139840003, -0.00200000009
827, 0.0143860001, -0.00200000009
828, 0.0147879999, -0.00200000009
829, 0.0151899997, -0.00200000009
830, 0.0155920004, -0.00200000009
831, 0.0159939993, -0.00200000009
832, 0.0163959991, -0.00200000009
833, 0.0167980008, -0.00200000009
834, 0.0135791432, -0.0017142857
835, 0.0139782857, -0.0017142857
836, 0.0143774282, -0.0017142857
837, 0.0147765717, -0.0017142857
838, 0.0151757142, -0.0017142857
839, 0.0155748576, -0.0017142857
840, 0.0159740001, -0.0017142857
841, 0.0163731426, -0.0017142857
842, 0.0167722851, -0.0017142857
843, 0.0135762859, -0.00142857141
844, 0.0139725711, -0.00142857141
845, 0.0143688573, -0.00142857141
846, 0.0147651425, -0.00142857141
847, 0.0151614286, -0.00142857141
848, 0.0155577147, -0.00142857141
849, 0.0159540009, -0.00142857141
850, 0.0163502861, -0.00142857141
851, 0.0167465713, -0.00142857141
852, 0.0135734286, -0.00114285713
853, 0.0139668575, -0.00114285713
854, 0.0143602854, -0.00114285713
855, 0.0147537142, -0.00114285713
856, 0.015147143, -0.00114285713
857, 0.0155405719, -0.00114285713
858, 0.0159339998, -0.00114285713
859, 0.0163274277, -0.00114285713
860, 0.0167208575, -0.00114285713
861, 0.0135705713, -0.000857142848
862, 0.0139611429, -0.000857142848
863, 0.0143517144, -0.000857142848
864, 0.0147422859, -0.000857142848
865, 0.0151328575, -0.000857142848
866, 0.015523429, -0.000857142848
867, 0.0159140006, -0.000857142848
868, 0.0163045712, -0.000857142848
869, 0.0166951437, -0.000857142848
870, 0.013567714, -0.000571428565
871, 0.0139554283, -0.000571428565
872, 0.0143431425, -0.000571428565

873, 0.0147308568, -0.000571428565
874, 0.015118571, -0.000571428565
875, 0.0155062862, -0.000571428565
876, 0.0158939995, -0.000571428565
877, 0.0162817147, -0.000571428565
878, 0.016669428, -0.000571428565
879, 0.0135648567, -0.000285714283
880, 0.0139497146, -0.000285714283
881, 0.0143345715, -0.000285714283
882, 0.0147194285, -0.000285714283
883, 0.0151042854, -0.000285714283
884, 0.0154891433, -0.000285714283
885, 0.0158740003, -0.000285714283
886, 0.0162588563, -0.000285714283
887, 0.0166437142, -0.000285714283
888, 0.00352542009, 0.0162397455
889, 0.00313873356, 0.0163188931
890, 0.00275027636, 0.0163888354
891, 0.00236026756, 0.0164495315
892, 0.00196892745, 0.0165009461
893, 0.0015764765, 0.016543055
894, 0.00118313625, 0.0165758301
895, 0.000789128477, 0.0165992528
896, 0.000394675561, 0.0166133121
897, 0.00344438083, 0.0158664398
898, 0.00306658307, 0.0159437694
899, 0.00268705538, 0.0160121024
900, 0.00230601197, 0.0160714034
901, 0.0019236675, 0.0161216371
902, 0.0015402378, 0.0161627773
903, 0.0011559393, 0.0161947981
904, 0.0007709887, 0.0162176844
905, 0.000385603111, 0.0162314195
906, 0.00336334156, 0.0154931359
907, 0.00299443258, 0.0155686447
908, 0.00262383441, 0.0156353712
909, 0.00225175614, 0.0156932753
910, 0.00187840755, 0.015742328
911, 0.00150399923, 0.0157824997
912, 0.00112874247, 0.0158137679
913, 0.000752848922, 0.0158361141
914, 0.000376530661, 0.0158495288
915, 0.00328230229, 0.0151198301
916, 0.00292228209, 0.0151935201
917, 0.00256061344, 0.0152586382
918, 0.00219750032, 0.015315149
919, 0.00183314749, 0.015363019
920, 0.00146776054, 0.015402223
921, 0.00110154552, 0.0154327378
922, 0.000734709087, 0.0154545456
923, 0.000367458211, 0.0154676363
924, 0.00320126303, 0.0147465253

925, 0.0028501316, 0.0148183955
926, 0.00249739271, 0.0148819061
927, 0.00214324472, 0.0149370208
928, 0.00178788754, 0.0149837099
929, 0.00143152184, 0.0150219453
930, 0.00107434869, 0.0150517067
931, 0.00071656931, 0.0150729772
932, 0.000358385732, 0.0150857437
933, 0.00312022376, 0.0143732205
934, 0.00277798134, 0.0144432709
935, 0.00243417174, 0.014505174
936, 0.0020889889, 0.0145588936
937, 0.00174262759, 0.0146044008
938, 0.00139528327, 0.0146416686
939, 0.00104715175, 0.0146706766
940, 0.000698429532, 0.0146914078
941, 0.000349313283, 0.0147038512
942, 0.00303918449, 0.0139999157
943, 0.00270583085, 0.0140681472
944, 0.00237095077, 0.0141284419
945, 0.00203473307, 0.0141807664
946, 0.00169736764, 0.0142250909
947, 0.00135904457, 0.014261391
948, 0.0010199548, 0.0142896455
949, 0.000680289755, 0.0143098384
950, 0.000340240833, 0.0143219586
951, 0.00295814523, 0.0136266109
952, 0.00263368036, 0.0136930225
953, 0.0023077298, 0.0137517098
954, 0.00198047725, 0.0138026392
955, 0.00165210757, 0.0138457818
956, 0.00132280588, 0.0138811134
957, 0.000992757967, 0.0139086153
958, 0.00066214992, 0.01392827
959, 0.000331168383, 0.013940067
960, 0.00287710596, 0.0132533051
961, 0.00256152987, 0.0133178979
962, 0.00224450883, 0.0133749777
963, 0.00192622154, 0.013424512
964, 0.00160684763, 0.0134664727
965, 0.00128656731, 0.0135008367
966, 0.000965561077, 0.0135275843
967, 0.000644010142, 0.0135467006
968, 0.000322095933, 0.0135581745
*Element, type=CAX4R
1, 1, 13, 231, 138
2, 13, 14, 232, 231
3, 14, 15, 233, 232
4, 15, 16, 234, 233
5, 16, 17, 235, 234
6, 17, 18, 236, 235
7, 18, 19, 237, 236

8, 19, 20, 238, 237
9, 20, 21, 239, 238
10, 21, 2, 22, 239
11, 138, 231, 240, 137
12, 231, 232, 241, 240
13, 232, 233, 242, 241
14, 233, 234, 243, 242
15, 234, 235, 244, 243
16, 235, 236, 245, 244
17, 236, 237, 246, 245
18, 237, 238, 247, 246
19, 238, 239, 248, 247
20, 239, 22, 23, 248
21, 137, 240, 249, 136
22, 240, 241, 250, 249
23, 241, 242, 251, 250
24, 242, 243, 252, 251
25, 243, 244, 253, 252
26, 244, 245, 254, 253
27, 245, 246, 255, 254
28, 246, 247, 256, 255
29, 247, 248, 257, 256
30, 248, 23, 24, 257
31, 136, 249, 258, 135
32, 249, 250, 259, 258
33, 250, 251, 260, 259
34, 251, 252, 261, 260
35, 252, 253, 262, 261
36, 253, 254, 263, 262
37, 254, 255, 264, 263
38, 255, 256, 265, 264
39, 256, 257, 266, 265
40, 257, 24, 25, 266
41, 135, 258, 267, 134
42, 258, 259, 268, 267
43, 259, 260, 269, 268
44, 260, 261, 270, 269
45, 261, 262, 271, 270
46, 262, 263, 272, 271
47, 263, 264, 273, 272
48, 264, 265, 274, 273
49, 265, 266, 275, 274
50, 266, 25, 26, 275
51, 134, 267, 276, 133
52, 267, 268, 277, 276
53, 268, 269, 278, 277
54, 269, 270, 279, 278
55, 270, 271, 280, 279
56, 271, 272, 281, 280
57, 272, 273, 282, 281
58, 273, 274, 283, 282
59, 274, 275, 284, 283

60, 275, 26, 27, 284
61, 133, 276, 285, 132
62, 276, 277, 286, 285
63, 277, 278, 287, 286
64, 278, 279, 288, 287
65, 279, 280, 289, 288
66, 280, 281, 290, 289
67, 281, 282, 291, 290
68, 282, 283, 292, 291
69, 283, 284, 293, 292
70, 284, 27, 28, 293
71, 132, 285, 294, 131
72, 285, 286, 295, 294
73, 286, 287, 296, 295
74, 287, 288, 297, 296
75, 288, 289, 298, 297
76, 289, 290, 299, 298
77, 290, 291, 300, 299
78, 291, 292, 301, 300
79, 292, 293, 302, 301
80, 293, 28, 29, 302
81, 131, 294, 303, 130
82, 294, 295, 304, 303
83, 295, 296, 305, 304
84, 296, 297, 306, 305
85, 297, 298, 307, 306
86, 298, 299, 308, 307
87, 299, 300, 309, 308
88, 300, 301, 310, 309
89, 301, 302, 311, 310
90, 302, 29, 30, 311
91, 130, 303, 312, 129
92, 303, 304, 313, 312
93, 304, 305, 314, 313
94, 305, 306, 315, 314
95, 306, 307, 316, 315
96, 307, 308, 317, 316
97, 308, 309, 318, 317
98, 309, 310, 319, 318
99, 310, 311, 320, 319
100, 311, 30, 31, 320
101, 129, 312, 321, 128
102, 312, 313, 322, 321
103, 313, 314, 323, 322
104, 314, 315, 324, 323
105, 315, 316, 325, 324
106, 316, 317, 326, 325
107, 317, 318, 327, 326
108, 318, 319, 328, 327
109, 319, 320, 329, 328
110, 320, 31, 32, 329
111, 128, 321, 330, 127

112, 321, 322, 331, 330
113, 322, 323, 332, 331
114, 323, 324, 333, 332
115, 324, 325, 334, 333
116, 325, 326, 335, 334
117, 326, 327, 336, 335
118, 327, 328, 337, 336
119, 328, 329, 338, 337
120, 329, 32, 33, 338
121, 127, 330, 339, 126
122, 330, 331, 340, 339
123, 331, 332, 341, 340
124, 332, 333, 342, 341
125, 333, 334, 343, 342
126, 334, 335, 344, 343
127, 335, 336, 345, 344
128, 336, 337, 346, 345
129, 337, 338, 347, 346
130, 338, 33, 34, 347
131, 126, 339, 348, 125
132, 339, 340, 349, 348
133, 340, 341, 350, 349
134, 341, 342, 351, 350
135, 342, 343, 352, 351
136, 343, 344, 353, 352
137, 344, 345, 354, 353
138, 345, 346, 355, 354
139, 346, 347, 356, 355
140, 347, 34, 35, 356
141, 125, 348, 357, 124
142, 348, 349, 358, 357
143, 349, 350, 359, 358
144, 350, 351, 360, 359
145, 351, 352, 361, 360
146, 352, 353, 362, 361
147, 353, 354, 363, 362
148, 354, 355, 364, 363
149, 355, 356, 365, 364
150, 356, 35, 36, 365
151, 124, 357, 366, 123
152, 357, 358, 367, 366
153, 358, 359, 368, 367
154, 359, 360, 369, 368
155, 360, 361, 370, 369
156, 361, 362, 371, 370
157, 362, 363, 372, 371
158, 363, 364, 373, 372
159, 364, 365, 374, 373
160, 365, 36, 37, 374
161, 123, 366, 375, 122
162, 366, 367, 376, 375
163, 367, 368, 377, 376

164, 368, 369, 378, 377
165, 369, 370, 379, 378
166, 370, 371, 380, 379
167, 371, 372, 381, 380
168, 372, 373, 382, 381
169, 373, 374, 383, 382
170, 374, 37, 38, 383
171, 122, 375, 384, 121
172, 375, 376, 385, 384
173, 376, 377, 386, 385
174, 377, 378, 387, 386
175, 378, 379, 388, 387
176, 379, 380, 389, 388
177, 380, 381, 390, 389
178, 381, 382, 391, 390
179, 382, 383, 392, 391
180, 383, 38, 39, 392
181, 121, 384, 393, 120
182, 384, 385, 394, 393
183, 385, 386, 395, 394
184, 386, 387, 396, 395
185, 387, 388, 397, 396
186, 388, 389, 398, 397
187, 389, 390, 399, 398
188, 390, 391, 400, 399
189, 391, 392, 401, 400
190, 392, 39, 40, 401
191, 120, 393, 402, 119
192, 393, 394, 403, 402
193, 394, 395, 404, 403
194, 395, 396, 405, 404
195, 396, 397, 406, 405
196, 397, 398, 407, 406
197, 398, 399, 408, 407
198, 399, 400, 409, 408
199, 400, 401, 410, 409
200, 401, 40, 41, 410
201, 119, 402, 411, 118
202, 402, 403, 412, 411
203, 403, 404, 413, 412
204, 404, 405, 414, 413
205, 405, 406, 415, 414
206, 406, 407, 416, 415
207, 407, 408, 417, 416
208, 408, 409, 418, 417
209, 409, 410, 419, 418
210, 410, 41, 42, 419
211, 118, 411, 420, 117
212, 411, 412, 421, 420
213, 412, 413, 422, 421
214, 413, 414, 423, 422
215, 414, 415, 424, 423

216, 415, 416, 425, 424
217, 416, 417, 426, 425
218, 417, 418, 427, 426
219, 418, 419, 428, 427
220, 419, 42, 43, 428
221, 117, 420, 429, 116
222, 420, 421, 430, 429
223, 421, 422, 431, 430
224, 422, 423, 432, 431
225, 423, 424, 433, 432
226, 424, 425, 434, 433
227, 425, 426, 435, 434
228, 426, 427, 436, 435
229, 427, 428, 437, 436
230, 428, 43, 44, 437
231, 116, 429, 438, 115
232, 429, 430, 439, 438
233, 430, 431, 440, 439
234, 431, 432, 441, 440
235, 432, 433, 442, 441
236, 433, 434, 443, 442
237, 434, 435, 444, 443
238, 435, 436, 445, 444
239, 436, 437, 446, 445
240, 437, 44, 45, 446
241, 115, 438, 447, 114
242, 438, 439, 448, 447
243, 439, 440, 449, 448
244, 440, 441, 450, 449
245, 441, 442, 451, 450
246, 442, 443, 452, 451
247, 443, 444, 453, 452
248, 444, 445, 454, 453
249, 445, 446, 455, 454
250, 446, 45, 46, 455
251, 114, 447, 456, 113
252, 447, 448, 457, 456
253, 448, 449, 458, 457
254, 449, 450, 459, 458
255, 450, 451, 460, 459
256, 451, 452, 461, 460
257, 452, 453, 462, 461
258, 453, 454, 463, 462
259, 454, 455, 464, 463
260, 455, 46, 47, 464
261, 113, 456, 465, 112
262, 456, 457, 466, 465
263, 457, 458, 467, 466
264, 458, 459, 468, 467
265, 459, 460, 469, 468
266, 460, 461, 470, 469
267, 461, 462, 471, 470

268, 462, 463, 472, 471
269, 463, 464, 473, 472
270, 464, 47, 48, 473
271, 112, 465, 474, 111
272, 465, 466, 475, 474
273, 466, 467, 476, 475
274, 467, 468, 477, 476
275, 468, 469, 478, 477
276, 469, 470, 479, 478
277, 470, 471, 480, 479
278, 471, 472, 481, 480
279, 472, 473, 482, 481
280, 473, 48, 49, 482
281, 111, 474, 483, 110
282, 474, 475, 484, 483
283, 475, 476, 485, 484
284, 476, 477, 486, 485
285, 477, 478, 487, 486
286, 478, 479, 488, 487
287, 479, 480, 489, 488
288, 480, 481, 490, 489
289, 481, 482, 491, 490
290, 482, 49, 50, 491
291, 110, 483, 492, 109
292, 483, 484, 493, 492
293, 484, 485, 494, 493
294, 485, 486, 495, 494
295, 486, 487, 496, 495
296, 487, 488, 497, 496
297, 488, 489, 498, 497
298, 489, 490, 499, 498
299, 490, 491, 500, 499
300, 491, 50, 51, 500
301, 109, 492, 501, 108
302, 492, 493, 502, 501
303, 493, 494, 503, 502
304, 494, 495, 504, 503
305, 495, 496, 505, 504
306, 496, 497, 506, 505
307, 497, 498, 507, 506
308, 498, 499, 508, 507
309, 499, 500, 509, 508
310, 500, 51, 52, 509
311, 108, 501, 510, 107
312, 501, 502, 511, 510
313, 502, 503, 512, 511
314, 503, 504, 513, 512
315, 504, 505, 514, 513
316, 505, 506, 515, 514
317, 506, 507, 516, 515
318, 507, 508, 517, 516
319, 508, 509, 518, 517

320, 509, 52, 53, 518
321, 107, 510, 519, 106
322, 510, 511, 520, 519
323, 511, 512, 521, 520
324, 512, 513, 522, 521
325, 513, 514, 523, 522
326, 514, 515, 524, 523
327, 515, 516, 525, 524
328, 516, 517, 526, 525
329, 517, 518, 527, 526
330, 518, 53, 54, 527
331, 106, 519, 528, 105
332, 519, 520, 529, 528
333, 520, 521, 530, 529
334, 521, 522, 531, 530
335, 522, 523, 532, 531
336, 523, 524, 533, 532
337, 524, 525, 534, 533
338, 525, 526, 535, 534
339, 526, 527, 536, 535
340, 527, 54, 55, 536
341, 105, 528, 537, 104
342, 528, 529, 538, 537
343, 529, 530, 539, 538
344, 530, 531, 540, 539
345, 531, 532, 541, 540
346, 532, 533, 542, 541
347, 533, 534, 543, 542
348, 534, 535, 544, 543
349, 535, 536, 545, 544
350, 536, 55, 56, 545
351, 104, 537, 546, 103
352, 537, 538, 547, 546
353, 538, 539, 548, 547
354, 539, 540, 549, 548
355, 540, 541, 550, 549
356, 541, 542, 551, 550
357, 542, 543, 552, 551
358, 543, 544, 553, 552
359, 544, 545, 554, 553
360, 545, 56, 57, 554
361, 103, 546, 555, 102
362, 546, 547, 556, 555
363, 547, 548, 557, 556
364, 548, 549, 558, 557
365, 549, 550, 559, 558
366, 550, 551, 560, 559
367, 551, 552, 561, 560
368, 552, 553, 562, 561
369, 553, 554, 563, 562
370, 554, 57, 58, 563
371, 102, 555, 564, 101

372, 555, 556, 565, 564
373, 556, 557, 566, 565
374, 557, 558, 567, 566
375, 558, 559, 568, 567
376, 559, 560, 569, 568
377, 560, 561, 570, 569
378, 561, 562, 571, 570
379, 562, 563, 572, 571
380, 563, 58, 59, 572
381, 101, 564, 573, 100
382, 564, 565, 574, 573
383, 565, 566, 575, 574
384, 566, 567, 576, 575
385, 567, 568, 577, 576
386, 568, 569, 578, 577
387, 569, 570, 579, 578
388, 570, 571, 580, 579
389, 571, 572, 581, 580
390, 572, 59, 60, 581
391, 100, 573, 582, 99
392, 573, 574, 583, 582
393, 574, 575, 584, 583
394, 575, 576, 585, 584
395, 576, 577, 586, 585
396, 577, 578, 587, 586
397, 578, 579, 588, 587
398, 579, 580, 589, 588
399, 580, 581, 590, 589
400, 581, 60, 61, 590
401, 99, 582, 591, 98
402, 582, 583, 592, 591
403, 583, 584, 593, 592
404, 584, 585, 594, 593
405, 585, 586, 595, 594
406, 586, 587, 596, 595
407, 587, 588, 597, 596
408, 588, 589, 598, 597
409, 589, 590, 599, 598
410, 590, 61, 62, 599
411, 98, 591, 600, 97
412, 591, 592, 601, 600
413, 592, 593, 602, 601
414, 593, 594, 603, 602
415, 594, 595, 604, 603
416, 595, 596, 605, 604
417, 596, 597, 606, 605
418, 597, 598, 607, 606
419, 598, 599, 608, 607
420, 599, 62, 63, 608
421, 97, 600, 609, 96
422, 600, 601, 610, 609
423, 601, 602, 611, 610

424, 602, 603, 612, 611
425, 603, 604, 613, 612
426, 604, 605, 614, 613
427, 605, 606, 615, 614
428, 606, 607, 616, 615
429, 607, 608, 617, 616
430, 608, 63, 64, 617
431, 96, 609, 618, 95
432, 609, 610, 619, 618
433, 610, 611, 620, 619
434, 611, 612, 621, 620
435, 612, 613, 622, 621
436, 613, 614, 623, 622
437, 614, 615, 624, 623
438, 615, 616, 625, 624
439, 616, 617, 626, 625
440, 617, 64, 65, 626
441, 95, 618, 627, 94
442, 618, 619, 628, 627
443, 619, 620, 629, 628
444, 620, 621, 630, 629
445, 621, 622, 631, 630
446, 622, 623, 632, 631
447, 623, 624, 633, 632
448, 624, 625, 634, 633
449, 625, 626, 635, 634
450, 626, 65, 66, 635
451, 94, 627, 636, 93
452, 627, 628, 637, 636
453, 628, 629, 638, 637
454, 629, 630, 639, 638
455, 630, 631, 640, 639
456, 631, 632, 641, 640
457, 632, 633, 642, 641
458, 633, 634, 643, 642
459, 634, 635, 644, 643
460, 635, 66, 67, 644
461, 93, 636, 645, 92
462, 636, 637, 646, 645
463, 637, 638, 647, 646
464, 638, 639, 648, 647
465, 639, 640, 649, 648
466, 640, 641, 650, 649
467, 641, 642, 651, 650
468, 642, 643, 652, 651
469, 643, 644, 653, 652
470, 644, 67, 68, 653
471, 92, 645, 654, 91
472, 645, 646, 655, 654
473, 646, 647, 656, 655
474, 647, 648, 657, 656
475, 648, 649, 658, 657

476, 649, 650, 659, 658
477, 650, 651, 660, 659
478, 651, 652, 661, 660
479, 652, 653, 662, 661
480, 653, 68, 69, 662
481, 91, 654, 663, 90
482, 654, 655, 664, 663
483, 655, 656, 665, 664
484, 656, 657, 666, 665
485, 657, 658, 667, 666
486, 658, 659, 668, 667
487, 659, 660, 669, 668
488, 660, 661, 670, 669
489, 661, 662, 671, 670
490, 662, 69, 70, 671
491, 90, 663, 672, 89
492, 663, 664, 673, 672
493, 664, 665, 674, 673
494, 665, 666, 675, 674
495, 666, 667, 676, 675
496, 667, 668, 677, 676
497, 668, 669, 678, 677
498, 669, 670, 679, 678
499, 670, 671, 680, 679
500, 671, 70, 71, 680
501, 89, 672, 681, 88
502, 672, 673, 682, 681
503, 673, 674, 683, 682
504, 674, 675, 684, 683
505, 675, 676, 685, 684
506, 676, 677, 686, 685
507, 677, 678, 687, 686
508, 678, 679, 688, 687
509, 679, 680, 689, 688
510, 680, 71, 72, 689
511, 88, 681, 690, 87
512, 681, 682, 691, 690
513, 682, 683, 692, 691
514, 683, 684, 693, 692
515, 684, 685, 694, 693
516, 685, 686, 695, 694
517, 686, 687, 696, 695
518, 687, 688, 697, 696
519, 688, 689, 698, 697
520, 689, 72, 73, 698
521, 87, 690, 699, 86
522, 690, 691, 700, 699
523, 691, 692, 701, 700
524, 692, 693, 702, 701
525, 693, 694, 703, 702
526, 694, 695, 704, 703
527, 695, 696, 705, 704

528, 696, 697, 706, 705
529, 697, 698, 707, 706
530, 698, 73, 74, 707
531, 86, 699, 708, 85
532, 699, 700, 709, 708
533, 700, 701, 710, 709
534, 701, 702, 711, 710
535, 702, 703, 712, 711
536, 703, 704, 713, 712
537, 704, 705, 714, 713
538, 705, 706, 715, 714
539, 706, 707, 716, 715
540, 707, 74, 75, 716
541, 85, 708, 84,   4
542, 708, 709, 83, 84
543, 709, 710, 82, 83
544, 710, 711, 81, 82
545, 711, 712, 80, 81
546, 712, 713, 79, 80
547, 713, 714, 78, 79
548, 714, 715, 77, 78
549, 715, 716, 76, 77
550, 716, 75,   3, 76
551,   5, 139, 717, 162
552, 139, 140, 718, 717
553, 140, 141, 719, 718
554, 141, 142, 720, 719
555, 142, 143, 721, 720
556, 143, 144, 722, 721
557, 144, 145, 723, 722
558, 145, 146, 724, 723
559, 146, 147, 725, 724
560, 147,   1, 148, 725
561, 162, 717, 726, 161
562, 717, 718, 727, 726
563, 718, 719, 728, 727
564, 719, 720, 729, 728
565, 720, 721, 730, 729
566, 721, 722, 731, 730
567, 722, 723, 732, 731
568, 723, 724, 733, 732
569, 724, 725, 734, 733
570, 725, 148, 149, 734
571, 161, 726, 735, 160
572, 726, 727, 736, 735
573, 727, 728, 737, 736
574, 728, 729, 738, 737
575, 729, 730, 739, 738
576, 730, 731, 740, 739
577, 731, 732, 741, 740
578, 732, 733, 742, 741
579, 733, 734, 743, 742

580, 734, 149, 150, 743
581, 160, 735, 159, 7
582, 735, 736, 158, 159
583, 736, 737, 157, 158
584, 737, 738, 156, 157
585, 738, 739, 155, 156
586, 739, 740, 154, 155
587, 740, 741, 153, 154
588, 741, 742, 152, 153
589, 742, 743, 151, 152
590, 743, 150, 6, 151
591, 8, 163, 744, 186
592, 163, 164, 745, 744
593, 164, 165, 746, 745
594, 165, 166, 747, 746
595, 166, 167, 748, 747
596, 167, 168, 749, 748
597, 168, 169, 750, 749
598, 169, 170, 751, 750
599, 170, 171, 752, 751
600, 171, 9, 172, 752
601, 186, 744, 753, 185
602, 744, 745, 754, 753
603, 745, 746, 755, 754
604, 746, 747, 756, 755
605, 747, 748, 757, 756
606, 748, 749, 758, 757
607, 749, 750, 759, 758
608, 750, 751, 760, 759
609, 751, 752, 761, 760
610, 752, 172, 173, 761
611, 185, 753, 762, 184
612, 753, 754, 763, 762
613, 754, 755, 764, 763
614, 755, 756, 765, 764
615, 756, 757, 766, 765
616, 757, 758, 767, 766
617, 758, 759, 768, 767
618, 759, 760, 769, 768
619, 760, 761, 770, 769
620, 761, 173, 174, 770
621, 184, 762, 183, 11
622, 762, 763, 182, 183
623, 763, 764, 181, 182
624, 764, 765, 180, 181
625, 765, 766, 179, 180
626, 766, 767, 178, 179
627, 767, 768, 177, 178
628, 768, 769, 176, 177
629, 769, 770, 175, 176
630, 770, 174, 10, 175
631, 9, 171, 771, 212

632, 171, 170, 772, 771
633, 170, 169, 773, 772
634, 169, 168, 774, 773
635, 168, 167, 775, 774
636, 167, 166, 776, 775
637, 166, 165, 777, 776
638, 165, 164, 778, 777
639, 164, 163, 779, 778
640, 163, 8, 187, 779
641, 212, 771, 780, 211
642, 771, 772, 781, 780
643, 772, 773, 782, 781
644, 773, 774, 783, 782
645, 774, 775, 784, 783
646, 775, 776, 785, 784
647, 776, 777, 786, 785
648, 777, 778, 787, 786
649, 778, 779, 788, 787
650, 779, 187, 188, 788
651, 211, 780, 789, 210
652, 780, 781, 790, 789
653, 781, 782, 791, 790
654, 782, 783, 792, 791
655, 783, 784, 793, 792
656, 784, 785, 794, 793
657, 785, 786, 795, 794
658, 786, 787, 796, 795
659, 787, 788, 797, 796
660, 788, 188, 189, 797
661, 210, 789, 798, 209
662, 789, 790, 799, 798
663, 790, 791, 800, 799
664, 791, 792, 801, 800
665, 792, 793, 802, 801
666, 793, 794, 803, 802
667, 794, 795, 804, 803
668, 795, 796, 805, 804
669, 796, 797, 806, 805
670, 797, 189, 190, 806
671, 209, 798, 807, 208
672, 798, 799, 808, 807
673, 799, 800, 809, 808
674, 800, 801, 810, 809
675, 801, 802, 811, 810
676, 802, 803, 812, 811
677, 803, 804, 813, 812
678, 804, 805, 814, 813
679, 805, 806, 815, 814
680, 806, 190, 191, 815
681, 208, 807, 816, 207
682, 807, 808, 817, 816
683, 808, 809, 818, 817

684, 809, 810, 819, 818
685, 810, 811, 820, 819
686, 811, 812, 821, 820
687, 812, 813, 822, 821
688, 813, 814, 823, 822
689, 814, 815, 824, 823
690, 815, 191, 192, 824
691, 207, 816, 825, 206
692, 816, 817, 826, 825
693, 817, 818, 827, 826
694, 818, 819, 828, 827
695, 819, 820, 829, 828
696, 820, 821, 830, 829
697, 821, 822, 831, 830
698, 822, 823, 832, 831
699, 823, 824, 833, 832
700, 824, 192, 193, 833
701, 206, 825, 834, 205
702, 825, 826, 835, 834
703, 826, 827, 836, 835
704, 827, 828, 837, 836
705, 828, 829, 838, 837
706, 829, 830, 839, 838
707, 830, 831, 840, 839
708, 831, 832, 841, 840
709, 832, 833, 842, 841
710, 833, 193, 194, 842
711, 205, 834, 843, 204
712, 834, 835, 844, 843
713, 835, 836, 845, 844
714, 836, 837, 846, 845
715, 837, 838, 847, 846
716, 838, 839, 848, 847
717, 839, 840, 849, 848
718, 840, 841, 850, 849
719, 841, 842, 851, 850
720, 842, 194, 195, 851
721, 204, 843, 852, 203
722, 843, 844, 853, 852
723, 844, 845, 854, 853
724, 845, 846, 855, 854
725, 846, 847, 856, 855
726, 847, 848, 857, 856
727, 848, 849, 858, 857
728, 849, 850, 859, 858
729, 850, 851, 860, 859
730, 851, 195, 196, 860
731, 203, 852, 861, 202
732, 852, 853, 862, 861
733, 853, 854, 863, 862
734, 854, 855, 864, 863
735, 855, 856, 865, 864

736, 856, 857, 866, 865
737, 857, 858, 867, 866
738, 858, 859, 868, 867
739, 859, 860, 869, 868
740, 860, 196, 197, 869
741, 202, 861, 870, 201
742, 861, 862, 871, 870
743, 862, 863, 872, 871
744, 863, 864, 873, 872
745, 864, 865, 874, 873
746, 865, 866, 875, 874
747, 866, 867, 876, 875
748, 867, 868, 877, 876
749, 868, 869, 878, 877
750, 869, 197, 198, 878
751, 201, 870, 879, 200
752, 870, 871, 880, 879
753, 871, 872, 881, 880
754, 872, 873, 882, 881
755, 873, 874, 883, 882
756, 874, 875, 884, 883
757, 875, 876, 885, 884
758, 876, 877, 886, 885
759, 877, 878, 887, 886
760, 878, 198, 199, 887
761, 200, 879, 76, 3
762, 879, 880, 77, 76
763, 880, 881, 78, 77
764, 881, 882, 79, 78
765, 882, 883, 80, 79
766, 883, 884, 81, 80
767, 884, 885, 82, 81
768, 885, 886, 83, 82
769, 886, 887, 84, 83
770, 887, 199, 4, 84
771, 1, 147, 888, 13
772, 147, 146, 889, 888
773, 146, 145, 890, 889
774, 145, 144, 891, 890
775, 144, 143, 892, 891
776, 143, 142, 893, 892
777, 142, 141, 894, 893
778, 141, 140, 895, 894
779, 140, 139, 896, 895
780, 139, 5, 213, 896
781, 13, 888, 897, 14
782, 888, 889, 898, 897
783, 889, 890, 899, 898
784, 890, 891, 900, 899
785, 891, 892, 901, 900
786, 892, 893, 902, 901
787, 893, 894, 903, 902

788, 894, 895, 904, 903
789, 895, 896, 905, 904
790, 896, 213, 214, 905
791, 14, 897, 906, 15
792, 897, 898, 907, 906
793, 898, 899, 908, 907
794, 899, 900, 909, 908
795, 900, 901, 910, 909
796, 901, 902, 911, 910
797, 902, 903, 912, 911
798, 903, 904, 913, 912
799, 904, 905, 914, 913
800, 905, 214, 215, 914
801, 15, 906, 915, 16
802, 906, 907, 916, 915
803, 907, 908, 917, 916
804, 908, 909, 918, 917
805, 909, 910, 919, 918
806, 910, 911, 920, 919
807, 911, 912, 921, 920
808, 912, 913, 922, 921
809, 913, 914, 923, 922
810, 914, 215, 216, 923
811, 16, 915, 924, 17
812, 915, 916, 925, 924
813, 916, 917, 926, 925
814, 917, 918, 927, 926
815, 918, 919, 928, 927
816, 919, 920, 929, 928
817, 920, 921, 930, 929
818, 921, 922, 931, 930
819, 922, 923, 932, 931
820, 923, 216, 217, 932
821, 17, 924, 933, 18
822, 924, 925, 934, 933
823, 925, 926, 935, 934
824, 926, 927, 936, 935
825, 927, 928, 937, 936
826, 928, 929, 938, 937
827, 929, 930, 939, 938
828, 930, 931, 940, 939
829, 931, 932, 941, 940
830, 932, 217, 218, 941
831, 18, 933, 942, 19
832, 933, 934, 943, 942
833, 934, 935, 944, 943
834, 935, 936, 945, 944
835, 936, 937, 946, 945
836, 937, 938, 947, 946
837, 938, 939, 948, 947
838, 939, 940, 949, 948
839, 940, 941, 950, 949

840, 941, 218, 219, 950
841, 19, 942, 951, 20
842, 942, 943, 952, 951
843, 943, 944, 953, 952
844, 944, 945, 954, 953
845, 945, 946, 955, 954
846, 946, 947, 956, 955
847, 947, 948, 957, 956
848, 948, 949, 958, 957
849, 949, 950, 959, 958
850, 950, 219, 220, 959
851, 20, 951, 960, 21
852, 951, 952, 961, 960
853, 952, 953, 962, 961
854, 953, 954, 963, 962
855, 954, 955, 964, 963
856, 955, 956, 965, 964
857, 956, 957, 966, 965
858, 957, 958, 967, 966
859, 958, 959, 968, 967
860, 959, 220, 221, 968
861, 21, 960, 230,   2
862, 960, 961, 229, 230
863, 961, 962, 228, 229
864, 962, 963, 227, 228
865, 963, 964, 226, 227
866, 964, 965, 225, 226
867, 965, 966, 224, 225
868, 966, 967, 223, 224
869, 967, 968, 222, 223
870, 968, 221, 12, 222
*Nset, nset=HemisphereSection, generate
  1, 968,   1
*Elset, elset=HemisphereSection, generate
  1, 870,   1
*Nset, nset=InternalSet
  2,   3,   9, 10, 12, 22, 23, 24, 25, 26, 27, 28, 29, 30, 31, 32
 33, 34, 35, 36, 37, 38, 39, 40, 41, 42, 43, 44, 45, 46, 47, 48
 49, 50, 51, 52, 53, 54, 55, 56, 57, 58, 59, 60, 61, 62, 63, 64
 65, 66, 67, 68, 69, 70, 71, 72, 73, 74, 75, 172, 173, 174, 200, 201
202, 203, 204, 205, 206, 207, 208, 209, 210, 211, 212, 222, 223, 224, 225, 226
227, 228, 229, 230
*Elset, elset=InternalSet
 10, 20, 30, 40, 50, 60, 70, 80, 90, 100, 110, 120, 130, 140, 150, 160
170, 180, 190, 200, 210, 220, 230, 240, 250, 260, 270, 280, 290, 300, 310, 320
330, 340, 350, 360, 370, 380, 390, 400, 410, 420, 430, 440, 450, 460, 470, 480
490, 500, 510, 520, 530, 540, 550, 600, 610, 620, 630, 631, 641, 651, 661, 671
681, 691, 701, 711, 721, 731, 741, 751, 761, 861, 862, 863, 864, 865, 866, 867
868, 869, 870
*Nset, nset=Symmetry
  5,   7, 12, 160, 161, 162, 213, 214, 215, 216, 217, 218, 219, 220, 221
*Elset, elset=Symmetry

```
 551, 561, 571, 581, 780, 790, 800, 810, 820, 830, 840, 850, 860, 870
*Nset, nset=ExternalSet
   1,   4,   6,   7,   8,  11,  85,  86,  87,  88,  89,  90,  91,  92,  93,  94
  95,  96,  97,  98,  99, 100, 101, 102, 103, 104, 105, 106, 107, 108, 109, 110
 111, 112, 113, 114, 115, 116, 117, 118, 119, 120, 121, 122, 123, 124, 125, 126
 127, 128, 129, 130, 131, 132, 133, 134, 135, 136, 137, 138, 148, 149, 150, 151
 152, 153, 154, 155, 156, 157, 158, 159, 184, 185, 186, 187, 188, 189, 190, 191
 192, 193, 194, 195, 196, 197, 198, 199
*Elset, elset=ExternalSet
   1,  11,  21,  31,  41,  51,  61,  71,  81,  91, 101, 111, 121, 131, 141, 151
 161, 171, 181, 191, 201, 211, 221, 231, 241, 251, 261, 271, 281, 291, 301, 311
 321, 331, 341, 351, 361, 371, 381, 391, 401, 411, 421, 431, 441, 451, 461, 471
 481, 491, 501, 511, 521, 531, 541, 560, 570, 580, 581, 582, 583, 584, 585, 586
 587, 588, 589, 590, 591, 601, 611, 621, 640, 650, 660, 670, 680, 690, 700, 710
 720, 730, 740, 750, 760, 770
*Elset, elset=_SurfInt_S2, internal
  10,  20,  30,  40,  50,  60,  70,  80,  90, 100, 110, 120, 130, 140, 150, 160
 170, 180, 190, 200, 210, 220, 230, 240, 250, 260, 270, 280, 290, 300, 310, 320
 330, 340, 350, 360, 370, 380, 390, 400, 410, 420, 430, 440, 450, 460, 470, 480
 490, 500, 510, 520, 530, 540, 550, 600, 610, 620, 630, 780, 790, 800, 810, 820
 830, 840, 850, 860, 870
*Elset, elset=_SurfInt_S3, internal
 621, 622, 623, 624, 625, 626, 627, 628, 629, 630, 861, 862, 863, 864, 865, 866
 867, 868, 869, 870
*Elset, elset=_SurfInt_S4, internal, generate
 591,  761,   10
*Surface, type=ELEMENT, name=SurfInt
_SurfInt_S2, S2
_SurfInt_S3, S3
_SurfInt_S4, S4
*Elset, elset=_SurfExt_S4, internal
   1,  11,  21,  31,  41,  51,  61,  71,  81,  91, 101, 111, 121, 131, 141, 151
 161, 171, 181, 191, 201, 211, 221, 231, 241, 251, 261, 271, 281, 291, 301, 311
 321, 331, 341, 351, 361, 371, 381, 391, 401, 411, 421, 431, 441, 451, 461, 471
 481, 491, 501, 511, 521, 531, 541, 591, 601, 611, 621
*Elset, elset=_SurfExt_S2, internal
 560, 570, 580, 590, 640, 650, 660, 670, 680, 690, 700, 710, 720, 730, 740, 750
 760, 770
*Elset, elset=_SurfExt_S3, internal, generate
 581,  590,    1
*Surface, type=ELEMENT, name=SurfExt
_SurfExt_S4, S4
_SurfExt_S2, S2
_SurfExt_S3, S3
** Section: PZT_Dilatancy
*Solid Section, elset=HemisphereSection, material="PZT Dilatancy"
,
*End Part
**
*Part, name=MetalCore
*End Part
**
```

```
**
** ASSEMBLY
**
*Assembly, name=Assembly
**
*Instance, name=MetalCore-1, part=MetalCore
       0.,       -0.12,          0.
*Node
     1,          0.,  0.119999997,          0.
*Nset, nset=MetalCore-1-RefPt_, internal
1,
*Nset, nset="Reference core"
 1,
*Surface, type=SEGMENTS, name=SurfCore
START,          0.,      0.13318
 CIRCL,      0.01318,        0.12,          0.,        0.12
 LINE,      0.01318,       0.115
 LINE, 0.0174000070747003,       0.115
 CIRCL,       0.0175, 0.1149000070747,       0.0174,       0.1149
 LINE,       0.0175,       0.103
 LINE,       0.0225,       0.103
 LINE,       0.0225,       0.093
 LINE,       0.0275,       0.093
 LINE,       0.0275,       0.088
 LINE,          0.,       0.088
*Rigid Body, ref node=MetalCore-1-RefPt_, analytical surface=SurfCore
*End Instance
**
*Instance, name=Hemisphere-1, part=Hemisphere
*End Instance
**
*End Assembly
**
** MATERIALS
**
**
**
*Material, name="PZT Dilatancy"
*Cap Plasticity
537000., 67.21,  0.75, 0.297,  0.01,    1.
*Cap Hardening
    800631.,   0.
    801817., 0.05
    805233.,  0.1
    815074., 0.15
    843422.,  0.2
    925081., 0.25
 1.16031e+06,  0.3
 1.83789e+06, 0.35
 3.78975e+06,  0.4
 4.49429e+06, 0.41
 5.36486e+06, 0.42
```

```
 6.44058e+06, 0.43
 7.76979e+06, 0.44
 9.41224e+06, 0.45
 1.14417e+07, 0.46
 1.39495e+07, 0.47
 1.70482e+07, 0.48
 2.08771e+07, 0.49
 2.56083e+07,  0.5
 3.14545e+07, 0.51
 3.86783e+07, 0.52
 4.76044e+07, 0.53
 5.86339e+07, 0.54
 7.22626e+07, 0.55
 8.91029e+07, 0.56
 1.09912e+08, 0.57
 1.35624e+08, 0.58
 1.67396e+08, 0.59
 2.06654e+08,  0.6
 2.55164e+08, 0.61
*Density
2754.,
*Elastic
 1.758e+09, 0.178
**
**
*Material, name="PZT Fracture"
*Cap Plasticity
 1.06e+06,  68.3,  0.75, 0.295,  0.01,    1.
*Cap Hardening
    800631.,   0.
    801817., 0.05
    805233.,  0.1
    815074., 0.15
    843422.,  0.2
    925081., 0.25
 1.16031e+06,  0.3
 1.83789e+06, 0.35
 3.78975e+06,  0.4
 4.49429e+06, 0.41
 5.36486e+06, 0.42
 6.44058e+06, 0.43
 7.76979e+06, 0.44
 9.41224e+06, 0.45
 1.14417e+07, 0.46
 1.39495e+07, 0.47
 1.70482e+07, 0.48
 2.08771e+07, 0.49
 2.56083e+07,  0.5
 3.14545e+07, 0.51
 3.86783e+07, 0.52
 4.76044e+07, 0.53
 5.86339e+07, 0.54
```

```
 7.22626e+07, 0.55
 8.91029e+07, 0.56
 1.09912e+08, 0.57
 1.35624e+08, 0.58
 1.67396e+08, 0.59
 2.06654e+08,  0.6
 2.55164e+08, 0.61
*Density
2754.,
*Elastic
 1.758e+09, 0.178
**
** INTERACTION PROPERTIES
**
*Surface Interaction, name="Friction 03"
1.,
*Friction, slip tolerance=0.005
 0.3,
*Surface Behavior, pressure-overclosure=HARD
*Surface Interaction, name="No friction"
1.,
*Friction
0.,
*Surface Behavior, pressure-overclosure=HARD
*Surface Interaction, name="No slip"
1.,
*Friction, rough
*Surface Behavior, pressure-overclosure=HARD
**
** BOUNDARY CONDITIONS
**
** Name: FixedReference Type: Displacement/Rotation
*Boundary
MetalCore-1."Reference core", 1, 1
MetalCore-1."Reference core", 2, 2
MetalCore-1."Reference core", 6, 6
** Name: Symmetry Type: Symmetry/Antisymmetry/Encastre
*Boundary
Hemisphere-1.Symmetry, XSYMM
**
** INTERACTIONS
**
** Interaction: Core - powder
*Contact Pair, interaction="Friction 03", type=SURFACE TO SURFACE, tracking=STATE, adjust=0.0
Hemisphere-1.SurfInt, MetalCore-1.SurfCore
** ----------------------------------------------------------------
**
** STEP: Loading
**
*Step, name=Loading, nlgeom=YES, inc=100000, unsymm=YES
*Static
0.0005, 1., 1e-07, 0.05
```

```
**
** LOADS
**
** Name: Pressure   Type: Pressure
*Dsload
Hemisphere-1.SurfExt, P, 2e+08
**
** OUTPUT REQUESTS
**
*Restart, write, frequency=0
**
** FIELD OUTPUT: ExternalCoord
**
*Output, field, frequency=99999
*Node Output, nset=Hemisphere-1.ExternalSet
COORD,
**
** FIELD OUTPUT: FieldOutputs
**
*Output, field, time interval=0.05, time marks=NO
*Node Output
CF, RF, U
*Element Output, directions=YES
EVOL, LE, PE, PEEQ, PEMAG, PEQC, S
*Contact Output
CDISP, CSTRESS
**
** HISTORY OUTPUT: H-Output-1
**
*Output, history, variable=PRESELECT
*End Step
** ----------------------------------------------------------------
**
** STEP: Unloading
**
*Step, name=Unloading, nlgeom=YES, inc=100000, unsymm=YES
*Static
0.05, 0.97, 1e-07, 0.05
**
** LOADS
**
** Name: Pressure   Type: Pressure
*Dsload
Hemisphere-1.SurfExt, P, 6e+06
**
** OUTPUT REQUESTS
**
*Restart, write, frequency=0
**
** FIELD OUTPUT: ExternalCoord
**
*Output, field, frequency=99999
```

```
*Node Output, nset=Hemisphere-1.ExternalSet
COORD,
**
** FIELD OUTPUT: FieldOutputs
**
*Output, field, time interval=0.05, time marks=NO
*Node Output
CF, RF, U
*Element Output, directions=YES
EVOL, LE, PE, PEEQ, PEMAG, PEQC, S
*Contact Output
CDISP, CSTRESS
**
** HISTORY OUTPUT: H-Output-1
**
*Output, history, variable=PRESELECT
*End Step
** ----------------------------------------------------------------
**
** STEP: Final unloading
**
*Step, name="Final unloading", nlgeom=YES, inc=10000, unsymm=YES
*Static
0.0001, 0.027, 1e-10, 0.001
**
** LOADS
**
** Name: Pressure   Type: Pressure
*Dsload
Hemisphere-1.SurfExt, P, 600000.
**
** OUTPUT REQUESTS
**
*Restart, write, frequency=0
**
** FIELD OUTPUT: ExternalCoord
**
*Output, field, frequency=99999
*Node Output, nset=Hemisphere-1.ExternalSet
COORD,
**
** FIELD OUTPUT: FieldOutputs
**
*Output, field, time interval=0.005, time marks=NO
*Node Output
CF, RF, U
*Element Output, directions=YES
EVOL, LE, PE, PEEQ, PEMAG, PEQC, S
*Contact Output
CDISP, CSTRESS
**
** HISTORY OUTPUT: H-Output-1
```

**
*Output, history, variable=PRESELECT
*End Step

SUPPLEMENTARY MATERIAL S2-macroField_DensityEVOL

```
from abaqusConstants import *
from odbAccess import *

# Instructions

# Change only the header with the name of the .odb file and the bulk density of the powder.
# Run this script in Abaqus CAE. Click in the menu File > Run script. Then select this file.
# The code will start doing the calculations for each frame. The progress will be shown at the botton of the Abaqus interface.
# After calculation is finished. Choose the created variable in the field variables list (where standard variables are shown: displacmente, strain, stress...)

# ******************************************************************************
# Modify the next variables accordingly:

odbPath = "PZT-S1-DilatancyHardening-Ext.odb"                    # path to output database
initialDensity = 3.70                                    # initial density of the part
# ******************************************************************************

if odbPath in session.odbs.keys():
   session.odbs[odbPath].close()

odb = session.openOdb(name=odbPath,readOnly=FALSE)
```

```
allSteps = session.odbData[odbPath].steps.keys()
for i in range(len(allSteps)):
        step = odb.steps[allSteps[i]]
        allFrames = session.odbData[odbPath].steps[allSteps[i]].frames.keys()
        if i==0:
                volumeinitial = step.frames[0].fieldOutputs['EVOL']
        for j in range(len(allFrames)):
                frame = step.frames[j]
                volume = frame.fieldOutputs['EVOL']
                DEFVOL =  log(volume/volumeinitial)
                Density = initialDensity*(volumeinitial/volume)
                newFieldDEFVOL = frame.FieldOutput(name='DEFVOL', description='Plastic vol
strain', field=DEFVOL)
                newFieldDensity = frame.FieldOutput(name='Density', description='Density',
field=Density)
                print 'stepName = ', allSteps[i], ' frameNumber = ', allFrames[j]


odb.save()
odb.close()
odb = session.openOdb(name=odbPath)
session.Viewport(name='Viewport: 1', origin=(0.0, 0.0), width=192.5,
   height=88.0)
session.viewports['Viewport: 1'].makeCurrent()
session.viewports['Viewport: 1'].maximize()
session.viewports['Viewport: 1'].setValues(displayedObject=odb)
```